# SUPPORTING INFORMATION

Isabel Abánades Lázaro,[a]* Jose M. Rodrigo-Muñoz,[b] Beatriz Sastre,[b] María Romero Ángel,[a] Carlos Martí-Gastaldo[a] and Victoria del Pozo[b]*

[a]Instituto de Ciencia Molecular (ICMol), Universitat de València, Catedrático José Beltrán Martínez nº 2, 46980 Paterna, Valencia, Spain.

E-mail: Isabel.abanades@uv.es

[b]Department of Immunology, Instituto de Investigación Sanitaria Fundación Jiménez Díaz, Universidad Autónoma de Madrid (IIS-FJD, UAM), and CIBER de Enfermedades Respiratorias (CIBERES), 28029 Madrid, Spain.

E-mail: VPozo@fjd.es

## Table of contents

## S.1. General Experimental Remarks

**Powder X-Ray Diffraction (PXRD):**PXRD patterns were collected in a PANalyticalX'Pert PRO diffractometer using copper radiation (Cu Kα = 1.5418 Å) with an X'Celerator detector, operating at 40 mA and 45 kV. Profiles were collected in the 3° < 2θ < 40° range with a step size of 0.017°. (University of Valencia)

**Thermogravimetric Analysis (TGA):** were carried out with a Mettler Toledo TGA/SDTA 851 apparatus between 25 and 800 °C under ambient conditions (10 °C·$min^{-1}$scan rate and an air flow of 9 mL·min−1). (University of Valencia)

**Nuclear Magnetic Resonance Spectroscopy (NMR):** NMR spectra were recorded on either a Bruker AVIII 300 MHz spectrometer and referenced to residual solvent peaks. (University of Valencia)

**Gas Uptake:** $N_2$ adsorption isotherms were carried out at 77 K on a witha Micromeritics 3Flex gas sorption analyser. Samples were degassed under vacuum at 120 °C for 24 h in a Multisorb station prior to analysis. BET surface areas, micropore surface areas and external surface areas were calculated from the isotherms using the MicroActive operating software. The pore size distributions were calculated using NLDFT oxide surface pore model within the MicroActive software, with no regularisation. (University of Valencia)

**Scanning Electron Microscopy (SEM) and single point energy-dispersive X-Ray analysis (EDX):** particle morphologies, dimensions and mapping were studied with a Hitachi S-4800 scanning electron microscope at an accelerating voltage of 20 kV, over metalized samples with a mixture of gold and palladium for 90 seconds. (University of Valencia)

**Fourier Transform Infrared Spectroscopy:** IR spectra of solids were collected using a Shimadzu Fourier Transform Infrared Spectrometer, FTIR-8400S, fitted with a Diamond ATR unit. (University of Valencia)

**Dynamic Light Scattering:** Colloidal analysis was performed by Dynamic Light Scattering (DLS) with a Zetasizer Ultra potential analyser equipped with Non-Invasive Backscatter optics (NIBS) and a 50 mW laser at 633 nm. (University of Valencia).

**Flow Cytometry (Immune System Response):** Measurements were performed using a BD FACS Canto II. The analysis was done using Infinicyt and Prism software. (Instituto de Investigación Sanitaria Fundación Jiménez Díaz)

**Luminometer:** Luminescence (lambda= 570 nm) was recorded using a TECAN InfiniteF200 Luminometer. (Instituto de Investigación Sanitaria Fundación Jiménez Díaz)

## S.2. Materials and Synthesis

All reagents were obtained from commercial sources and were used without further purification.

### General remarks

In all syntheses, the jars were placed in an oven at room temperature and heated to 120℃ with 2℃/min ramp. The temperature was maintained for 24 hours and cooled down to room temperature with 0.4℃/min ramp. The resultant powder was collected by centrifugation (5000 rpm, 5 min) and washed with DMF (X2) and EtOH (x3) through dispersion-centrifugation cycles. The samples were dried under vacuum overnight and further activated by soxhlet with EtOH for approximately 24 hours. The samples were further dried under vacuum for 24 hours before characterization.

**Synthetic procedure for MUV-10:** In 25 mL pyrex jars, $CaCl_2$ (1 equivalent) was dissolved in 2 mL of solvent mixture. In a separate vial, BTC (1.5 equivalents), was dissolved in 9.8 mL of solvent mixture. The BTC solution was added to the $CaCl_2$ containing jar and the mixture was gently stirred, followed by slow Ti(IV) isopropoxide addition (1 equivalent compared to $CaCl_2$) and gentle stirring (See **Table S.X** samples for detailed values for Ca, Ti and BTC). In the unmodulated syntheses where no AcOH is used, the same amount of final volume is reached with DMF as the only solvent. If the synthetic conditions involve the use of HCl instead of AcOH (the same volume of HCl, 2.2 mL) is added to the BTC/$CaCl_2$ mixture prior to Ti(IV) isopropoxide addition**.**

**Table S1:** Tabulated general synthetic conditions of MUV-10

| Samples | $CaCl_2$ Mass/ mmol | $Ti(OiPr)_4$ µL/ mmol | BTC Mass/ mmol | Volume DMF | Equivalents of BTC Vs each metal | Modulator |
|---|---|---|---|---|---|---|
| **MUV-1720 nm** | 66 mg 0.6 mmol | 177.6 µL 0.6 mmol | 189 mg 0.9 mmol | 9.6 mL | 1.5 | HCl 2.2 mL |
| **MUV-135 nm** | 66 mg 0.6 mmol | 177.6 µL 0.6 mmol | 126 mg 0.6 mmol | 11.3 mL | l | AcOH 0.5 mL |
| **MUV-56 nm** | 66 mg 0.6 mmol | 177.6 µL 0.6 mmol | 189 mg 0.9 mmol | 11.6 mL | 1.5 | AcOH 0.2 mL |
| **MUV-28 nm** | 66 mg 0.6 mmol | 177.6 µL 0.6 mmol | 189 mg 0.9 mmol | 11.8 mL | 1.5 | n/a |

**Calcein Loading**

60 mg of MOF were dispersed by sonication (15 minutes) in 10 mL of ethanol solution of calcein (2 mg/mL) and stirred at room temperature for 48 hours. The solid was collected by centrifugation (4500 rpm, 5 min), and submitted to dispersion centrifugation cycles with fresh ethanol until the supernatant solution remained colourless (around 5 times). The calcein loaded materials were obtainedas bright orange powders.

**Dynamic Light Scattering (DLS) Measurements**

The particle size, aggregation and colloidal dispersion were measured by dynamic light scattering (DLS) in water and in phosphate-buffered saline (PBS) 10X. In a scintillation vial, dispersions of the samples with a concentration of 0.25 $mgmL^{-1}$ were prepared by sonication over 5 minutes before measurement.

**Degradation profiles**

To obtain the degradation profile of the different MOFs, around 3 mg of sample was dispersed in 15 mL of phosphate-buffered saline (PBS) 10X at pH 7.4 and stirred at room temperature. The release of the BTC linker, indicative of degradation, was measured by UV-Vis spectroscopy of an aliquot of supernatant. Prior to measurement, the samples were centrifuged. After the supernatant was measured by UV-vis (200-335 nm), the liquid was placed back to the degradation media prior to further measurement. For every measurement, the absorbance of the PBS blank was subtracted from the linker absorbance. The quantity of BTC (% *w/w*) present in the different samples was calculated based on the TGA measurements.

**Calcein release profiles**

To obtain the degradation profile of the different MOFs, around 3 mg of sample was dispersed in 15 mL of phosphate-buffered saline (PBS) 10X at pH 7.4 and stirred at room temperature. The release of the Calcein was measured by UV-Vis spectroscopy of an aliquot of supernatant using a 96-well plate with 50µL of supernatant diluted to 200 µL with PBS 10X. Prior to measurement, the samples were centrifuged. After the supernatant was measured by UV-vis (200-800 nm). For every measurement, the absorbance of the PBS blank was subtracted from the linker absorbance. The quantity of Calcein (% *w/w*) present in the different samples was calculated based on digested UV-Vis determination and TGA measurements.

## S.3. *In vitro* Protocols

### S3.1. Cell Culture

**J774 mouse monocyte-macrophage cell line** was cultured in RMPI-1640 medium supplemented with 0.1 mM nonessential amino acids, 100 units$mL^{-1}$ penicillin, 100 µg$mL^{-1}$ streptomycin, 10 mM HEPES, 2 mM L-glutamine, and 10% (*v/v*) fetal bovine serum and passaged twice a week (at 75-80% of confluence) at a density of 2.8 x $10^4$ cell$cm^{-2}$.

**Human peripheral blood mononuclear cells (PBMCs)** were isolated by gradient centrifugation on Lympoprep from the blood of five donors. After washes in RPMI 1640, the PBMCs were resuspended in completed RPMI supplemented as described above and were employed to analyze reactive oxygen species and for MTT assays. The culture cells were maintained at 37 ºC in a 5% $CO_2$ atmosphere.

### S3.2. Cytotoxicity Assays

The sample's cytotoxicity was measured against different cells in order to evaluate their effect on healthy cell proliferation.

To measure cell proliferation in the macrophage cell line J744 or in PBMCs isolated from the blood of donors, the cell proliferation kit I MTT (Roche), based on the cleavage of the tetrazolium salt 3-(4,5-dimethylthiazol-2-yl)-2,5-diphenyltetrazolium bromide, was used. J774 cells at 4 x $10^4$ (100 µl) and 1 x $10^5$ PBLs (100 µl) were cultured with different doses of NMOFs previously suspended in RPMI 1640 complete medium. J774 and PBM cells were incubated with nanoparticles for 24 h and for 72 hours. After that, 3-(4,5-dimethylthiazol-2-yl)-2,5-diphenyltetrazolium bromide (MTT) reagent (10 µl) per well was added. After 4 h of incubation in 5% $CO_2$ at 37 ºC with MTT reagent, 100 µl of MTT solubilisation buffer were added, followed by overnight incubation. Finally absorbance ($\lambda$ = 570 nm) was measured in a TECAN Infinite F200. Results were expressed as mean ± standard error of the mean of three experiments performed on different days, each of them with n = 3 unless otherwise stated. The average of the absorbance obtained for each concentration of each nanoparticle was compared with untreated cells.

### S3.3. J744 Macrophages and PBM cells Internalisation

Initially, the uptake of the calcein-loaded MOFs by the J774 macrophage or PBM cells was monitored by flow cytometry, to confirm that internalisation occurs and help rationalise any cytotoxicity. 5 x $10^5$ J774 cells per well were cultured with the different cal@MOFs at 250 µg/mL concentration for 2 h in 5% $CO_2$ and 37 ºC. Cells were recollected, washed with PBS and resuspended in FACs Flow and analysed by flow cytometry. Ratio of the mean fluorescence intensity (MFI) between cells cultured with nanoparticles and cultured with medium alone was analysed to determine the cell uptake ratio for each MOF in triplicate (n = 3).

### S3.4. Reactive Oxygen Species (ROS) Production

Five hundred thousand (500.000) J774 cells were cultured with 250 µg/mL of MOFs in RPMI complete medium without phenol red for 2 h in 5% $CO_2$ at 37 ºC (n=3). Then, 500 µl of PBS and 0.25 µl of the intracellular fluorescent probe $H_2$DC-FDA (20 mM probe, 5 mM final concentration) were added. After incubation, cells were recollected and washed with PBS. Cells were resuspended in FACS Flow and analysed by flow cytometry in a BD FACS Canto II flow cytometer, analysing the intracellular probe fluorescence. The ratio of the mean fluorescence intensity (MFI) between cells cultured with nanoparticles and cells cultured with medium alone was analysed.

### S3.5. Activation complement cascade

The effect of different MOFs in complement activation was carried out using serum from three donors. Serum (270 µl) were mixed with 250 µg/mL of MOFs dispersed in phosphate buffered saline (PBS). Complement proteins (C3 and C4) were analysed by immunoturbidimetric assay (absorbance at 340/694 nm) with specific antibodies against C3 and C4 (ADVIA Chemistry Systems, Siemens Healthcare Diagnostics Inc. Erlangen, Germany)

## S.4. Characterisation of empty samples

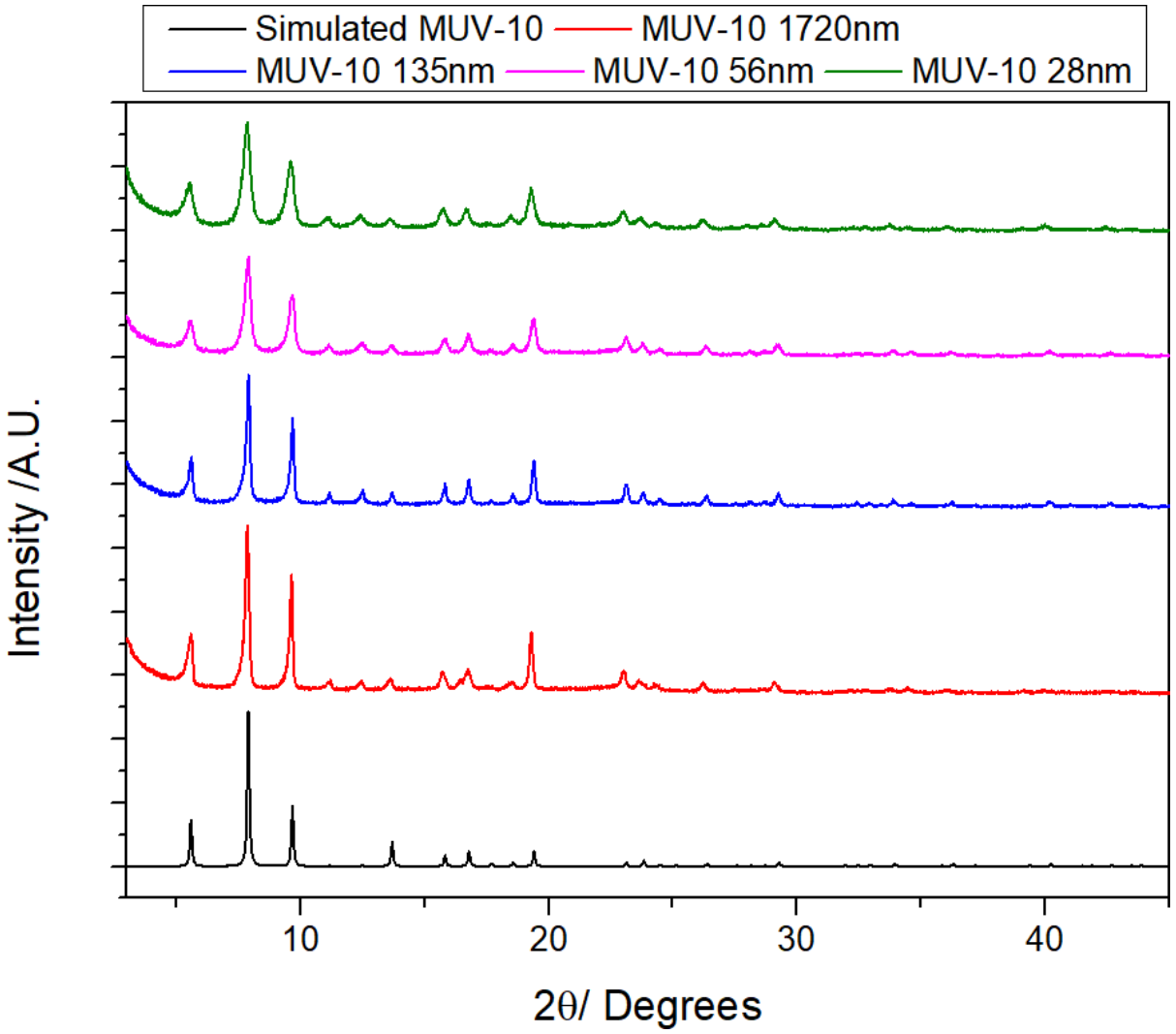


**Figure S1:** PXRD patterns of MUV-10 synthesized under different conditions, showing that phase pure MUV-10 is obtained under the different synthetic conditions. The reflection peaks are broader in agreement with the particle size decrease.

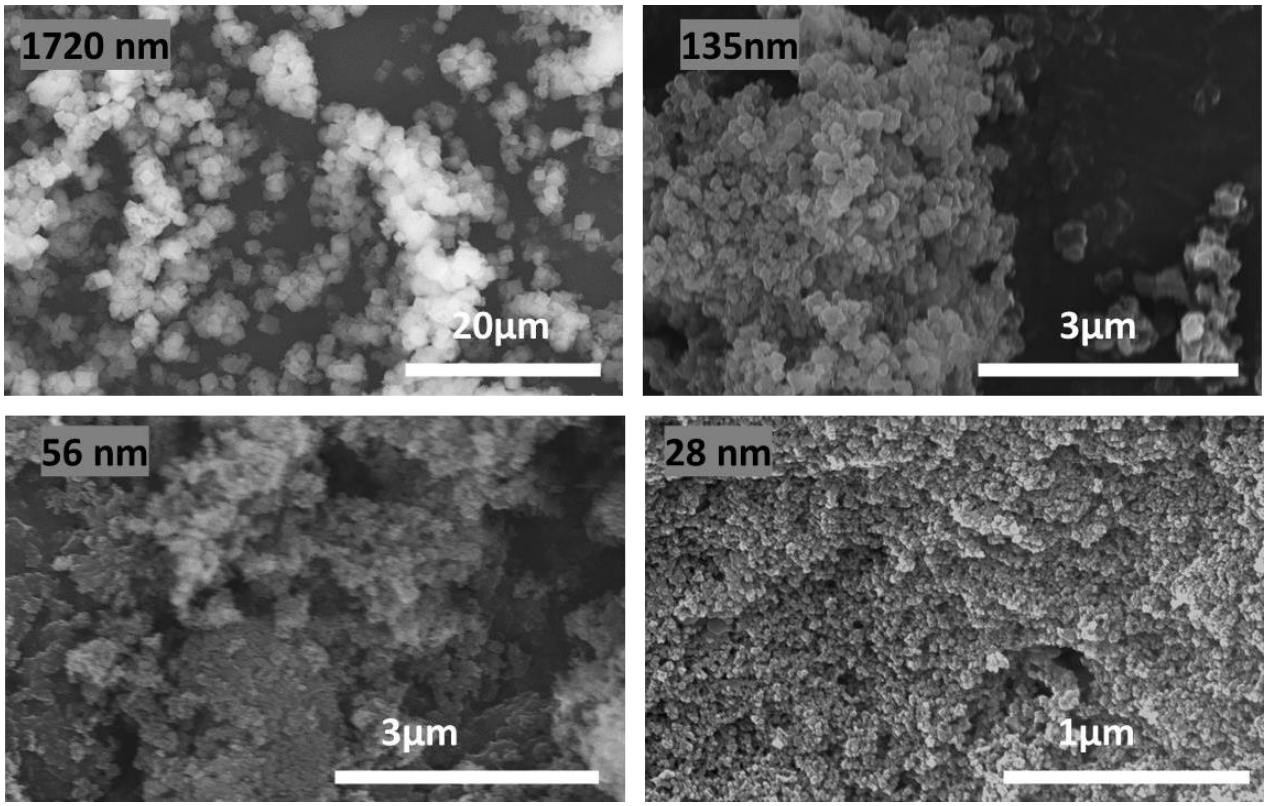


**Figure S2:**SEM images of MUV-10 synthesized under different conditions.

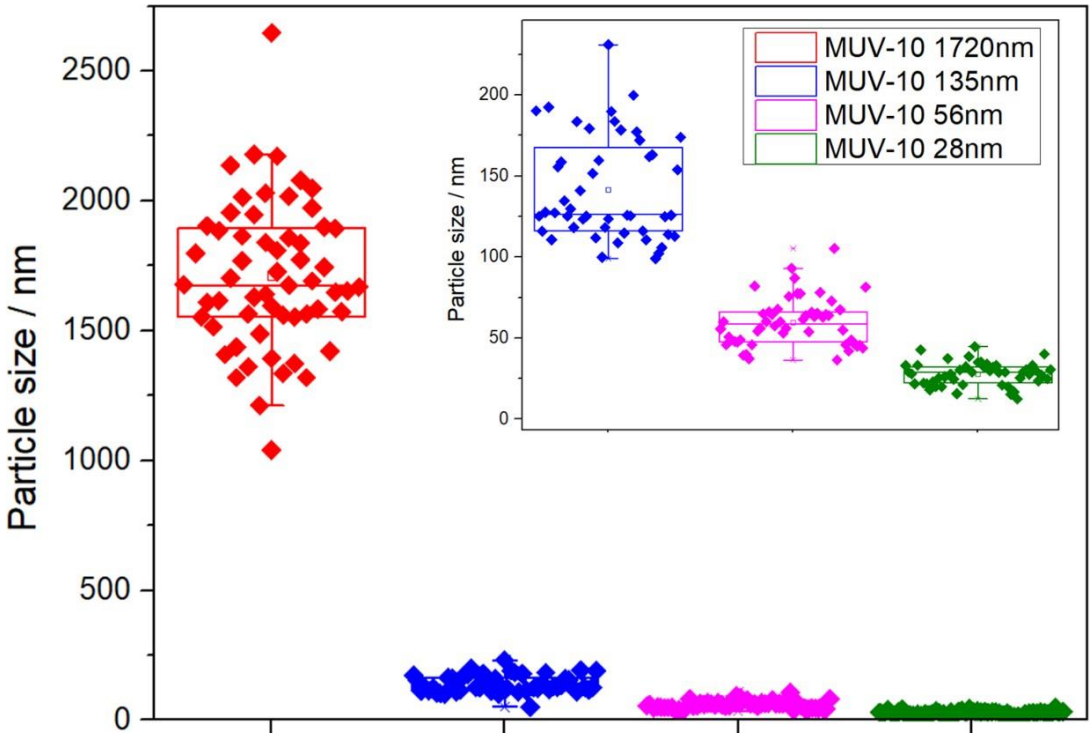


**Figure S3:** Box chart representation of MUV-10 particle sizes. Bin size of 10 nm.

**Table S2:** Tabulated particle sizes and Calcium content versus Titanium (Ca/(Ca+Ti)*100) of MUV-10 samples.

| **Sample** | **Size / nm** | **SD /nm** | **%Ca Vs Ti** |
|---|---|---|---|
| **1720 nm** | 1720 | 280 | 48.18 |
| **135 nm** | 135.6 | 34.3 | 43.26 |
| **56 nm** | 56.6 | 13.6 | 41.78 |
| **28 nm** | 28.1 | 7.7 | 46.73 |

**Table S3:**MOFs composition analysed by acid-digested $^{1}$HNMR.

| **Sample** | **FA/BTC** | **FA mol%** | **ACOH/BTC** | **AcOH mol%** | **DMF/BTC** |
|---|---|---|---|---|---|
| **1720 nm** | 0.023 | 0.022 | 0 | 0 | 0.592 |
| **135 nm** | 0.089 | 0.082 | 0.017 | 1.670 | 0.171 |
| **56 nm** | 0.068 | 0.064 | 0.009 | 0.910 | 0.176 |
| **28 nm** | 0.045 | 0.0431 | 0 | 0 | 0.089 |

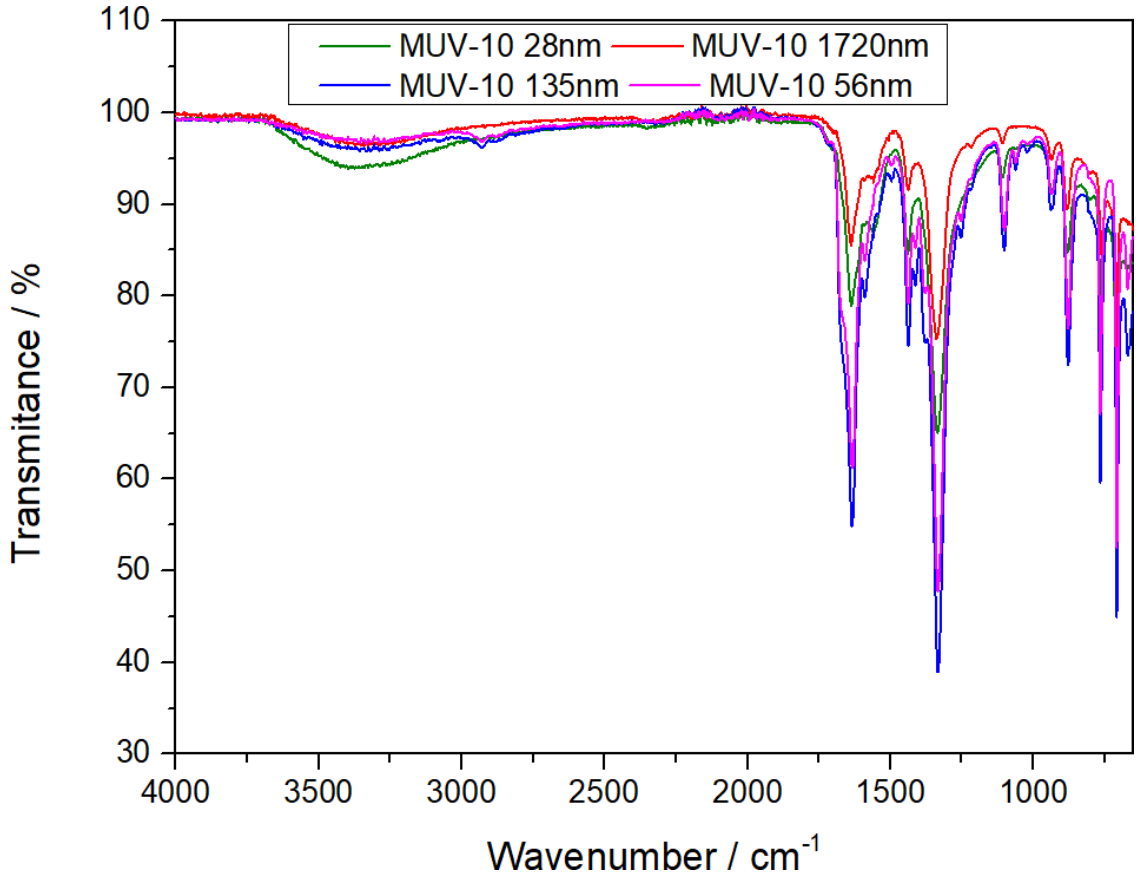


**Figure S4:**FT-IR profiles of MUV-10 synthesized under different conditions, showing that phase pure MUV-10 is obtained under the different synthetic conditions.

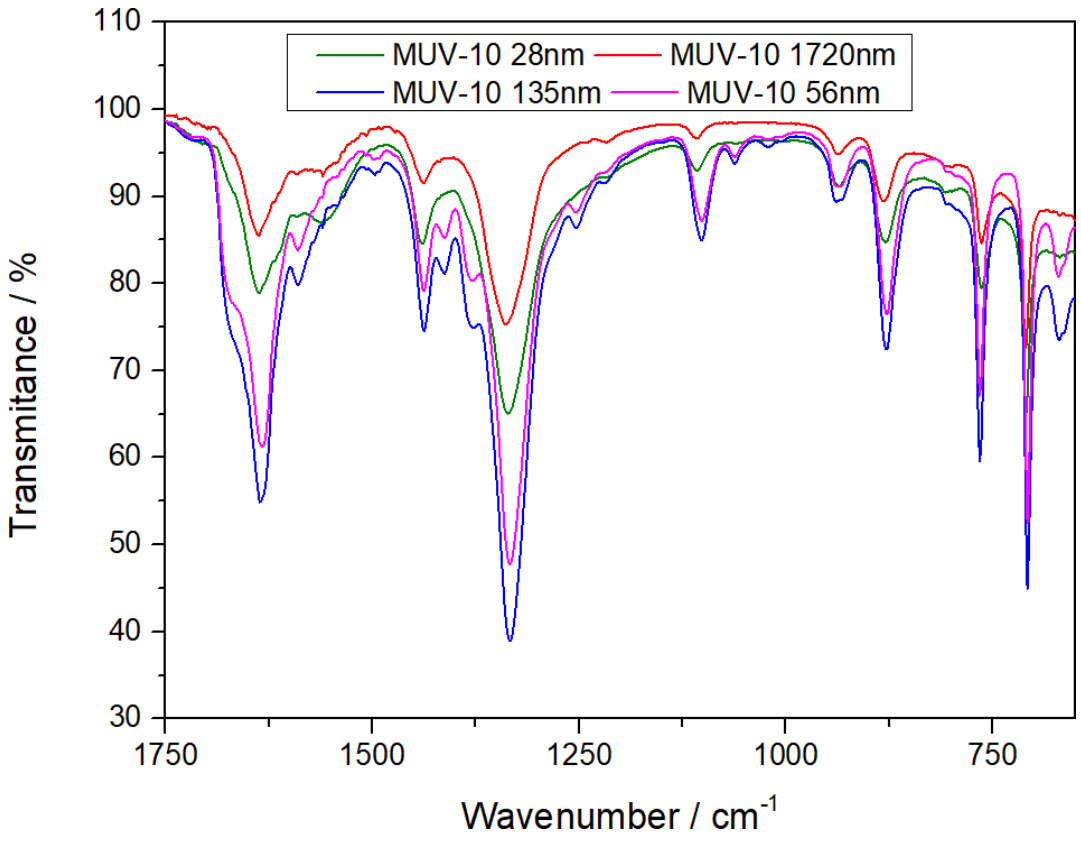


**Figure S5:**Magnification of the FT-IR profiles of MUV-10 synthesized under different conditions, showing changes in the carboxylate and metal vibration bands.

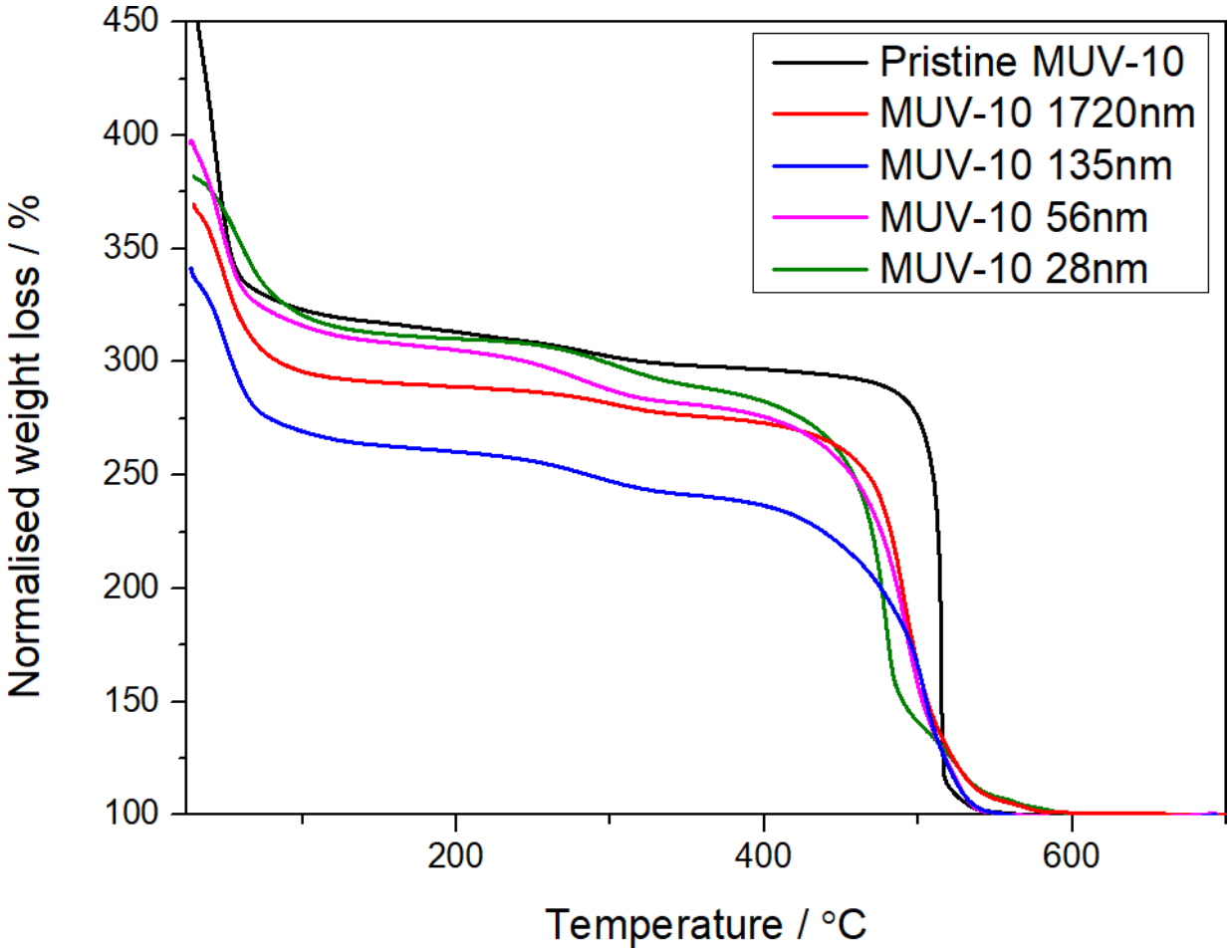


**Figure S6:** TGA profiles of MUV-10, compared to pristine MUV-10. The BTC decomposition step decreases while the defect-compensating step at 200-400ºC increases. All the samples show great thermal stability, and the BTC decrease is more significant for the sample synthesised with a lower quantity of linker.

**Table S4:** Tabulated data extracted from TGA[1,2]

| Sample | Ratio BTC/TI | FA | ACOH | OH | H2O | ML% | Coordination positions |
|---|---|---|---|---|---|---|---|
| **1720 nm** | 1.269 | 0.019 | 0.000 | 0.173 | 1.1 | 4.799 | 11.96 |
| **135 nm** | 1.019 | 0.091 | 0.017 | 0.834 | 0.7 | 23.548 | 10.87 |
| **56 nm** | 1.263 | 0.086 | 0.011 | 0.112 | 1.1 | 5.250 | 12.00 |
| **28 nm** | 1.232 | 0.047 | 0.000 | 0.256 | 2.8 | 7.583 | 13.51 |

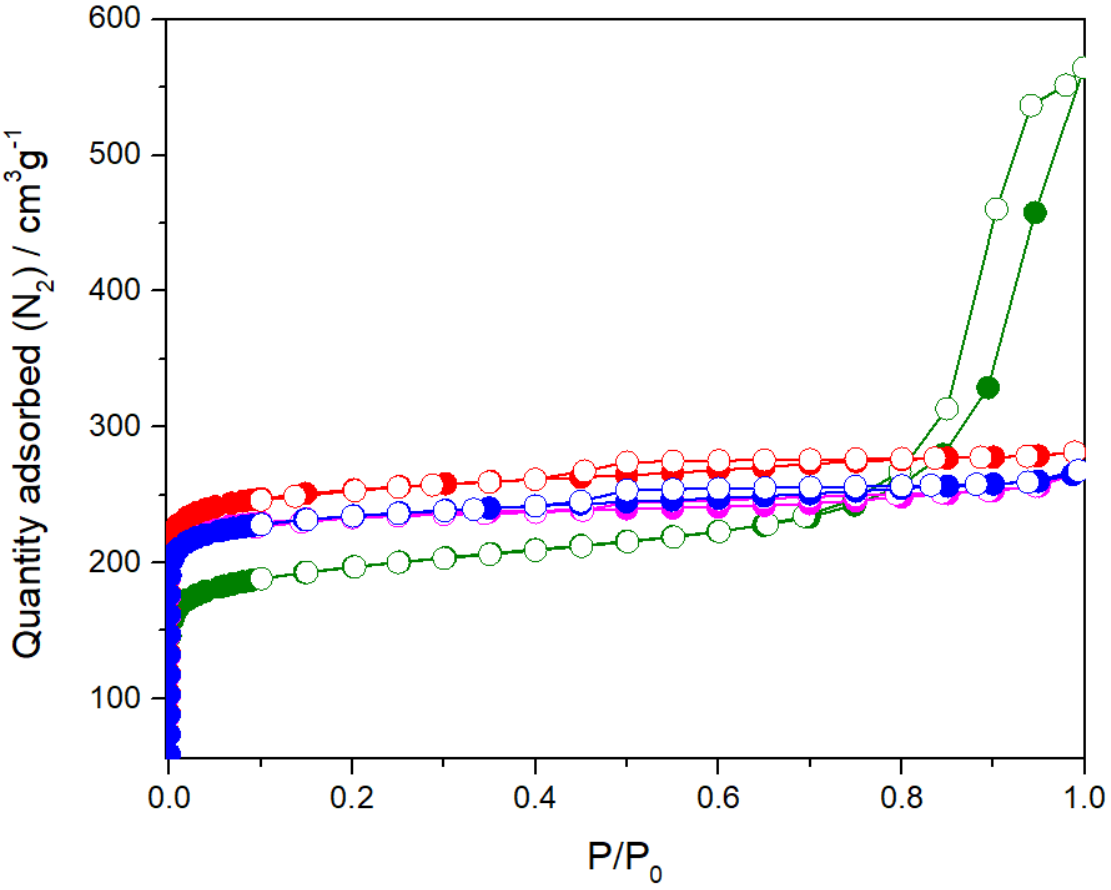


**Figure S7:** $N_2$ adsorption and desorption isotherms of MUV-10. The samplewith the smallest particle size shows mesoporosity coming from interparticle space.

**Table S5:**Porosimetry data of MUV-10 extracted from the N2 adsorption and desorption isotherms.

| Sample | $S_{BET}$ | $S_{MICRO}$ | $S_{EXT}$ | $V_{MICRO}$ | $V_{MESO}$ | $V_{TOTAL}$ | %$S_{EXT}$ | %$V_{MESO}$ |
|---|---|---|---|---|---|---|---|---|
| **1720 nm** | 1003 | 887 | 116 | 0.341 | 0.09 | 0.431 | 11.57 | 20.88 |
| **135 nm** | 929 | 830 | 99 | 0.319 | 0.078 | 0.397 | 10.66 | 19.65 |
| **56 nm** | 914 | 788 | 126 | 0.307 | 0.096 | 0.403 | 13.79 | 23.82 |
| **28 nm** | 751 | 558 | 193 | 0.221 | 0.289 | 0.510 | 25.70 | 56.67 |

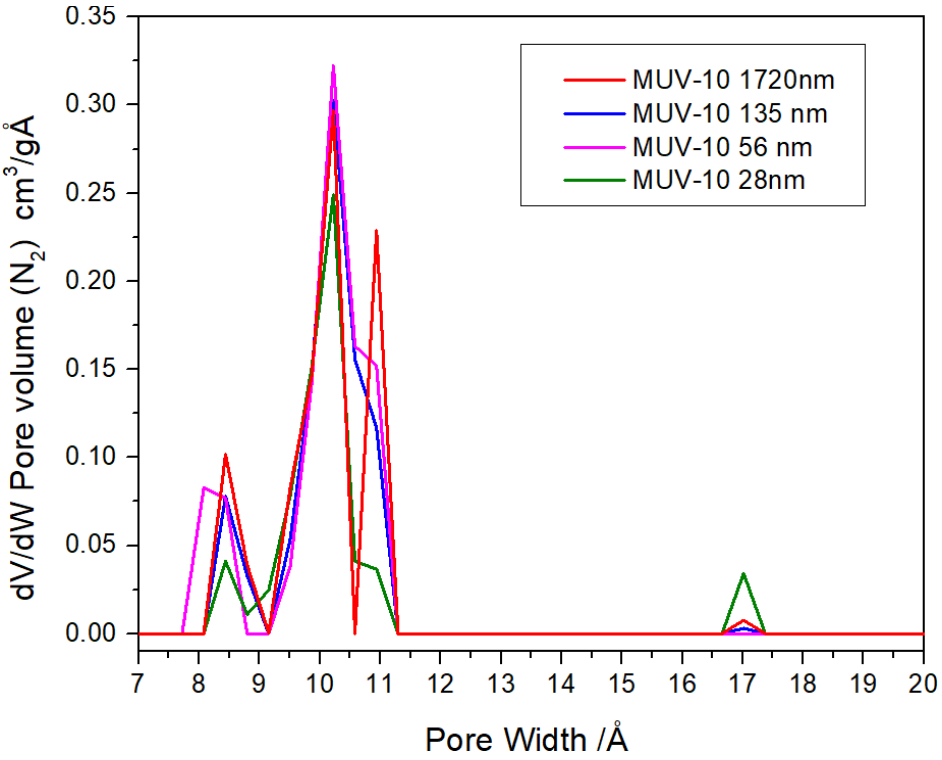


**Figure S8:** Pore size distribution of MUV-10, showing similar micropores for all the samples in great agreement with the reported MUV-10 micropore, and the appearance of bigger pores, possibly consequence of their defectivity.

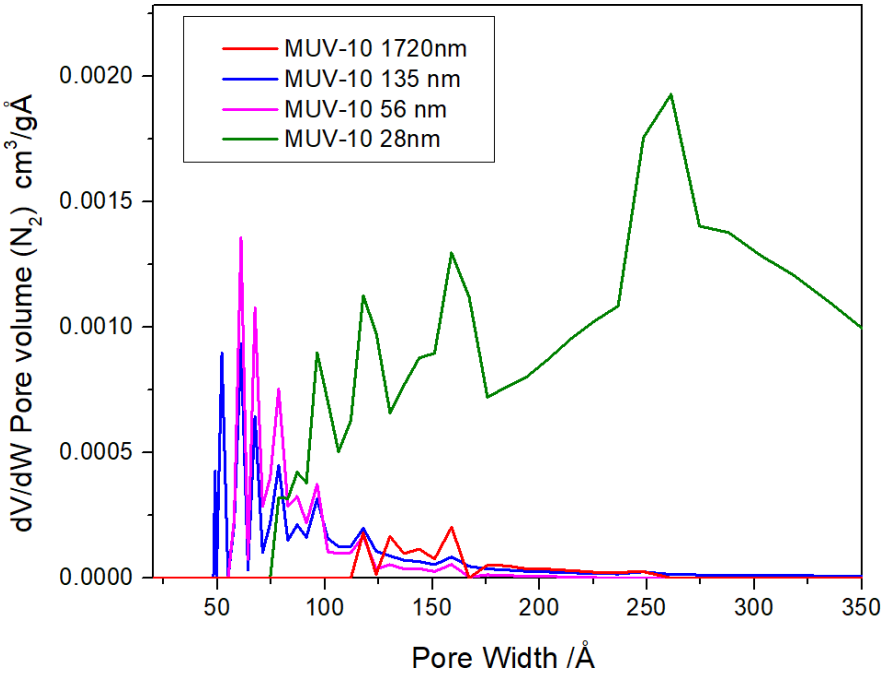


**Figure S9:** Pore size distribution of MUV-10, showing mesoporosity for the particles with smaller particle sizes, most likely coming from interparticle space.

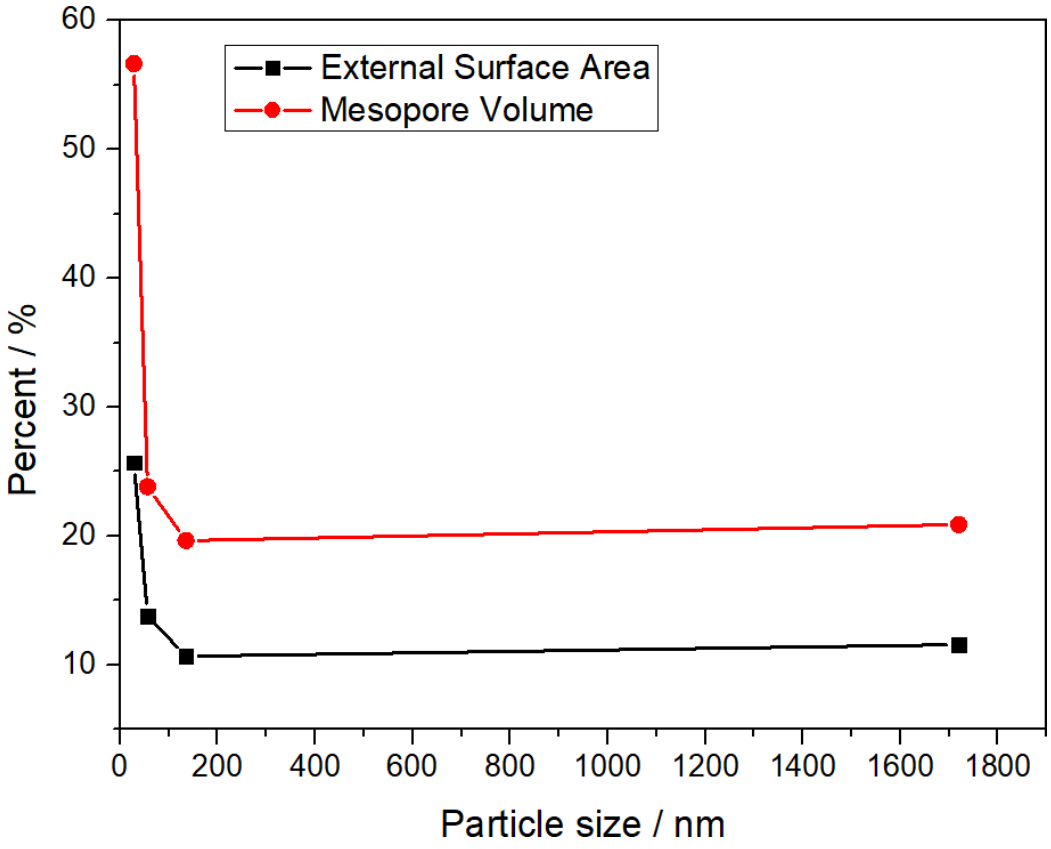


**Figure S10:** Relation between the external surface area and mesopore volume with the particle size.

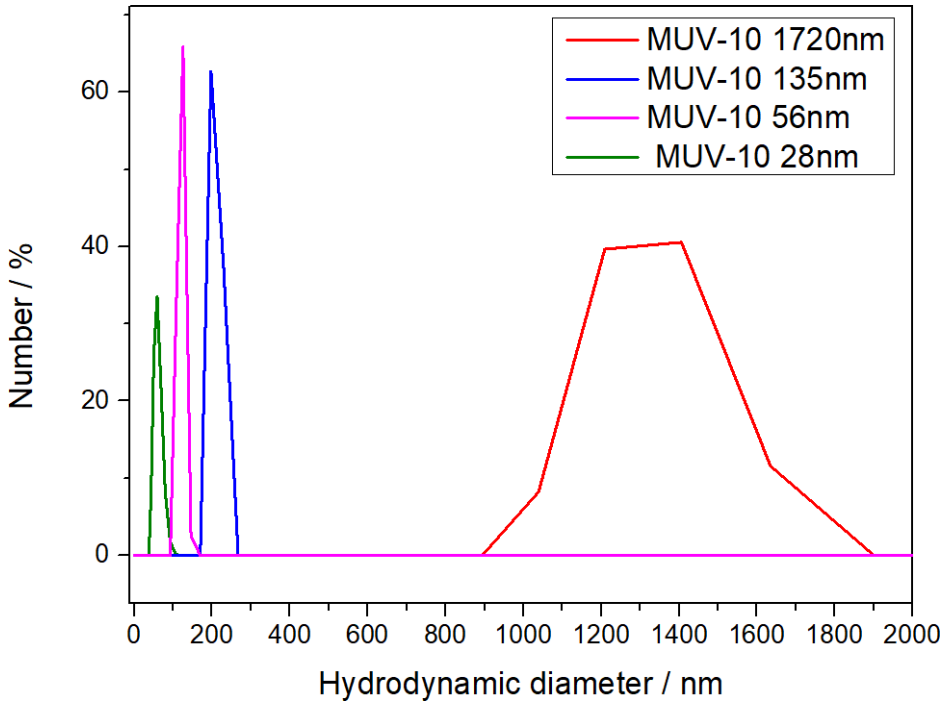


**Figure S11:** DLS measurements in PBS 10X.

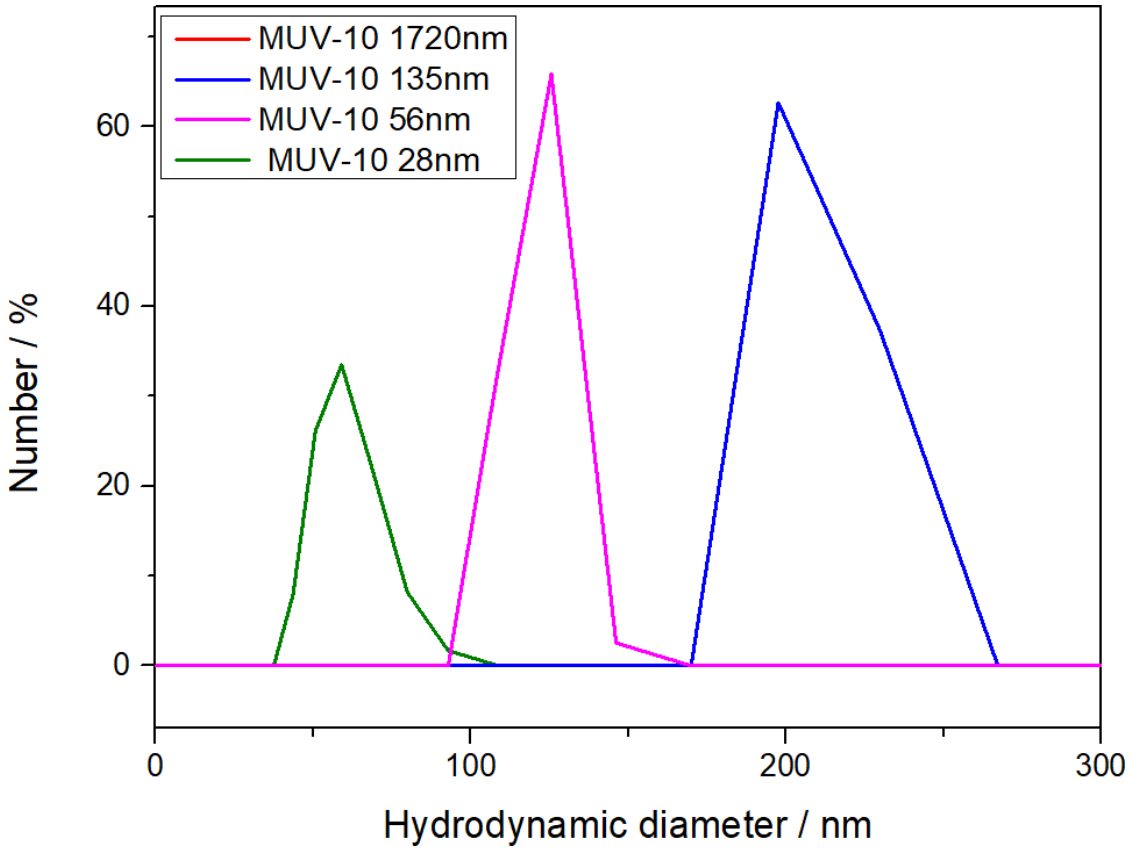


**Figure S12:** DLS measurements in PBS 10X.

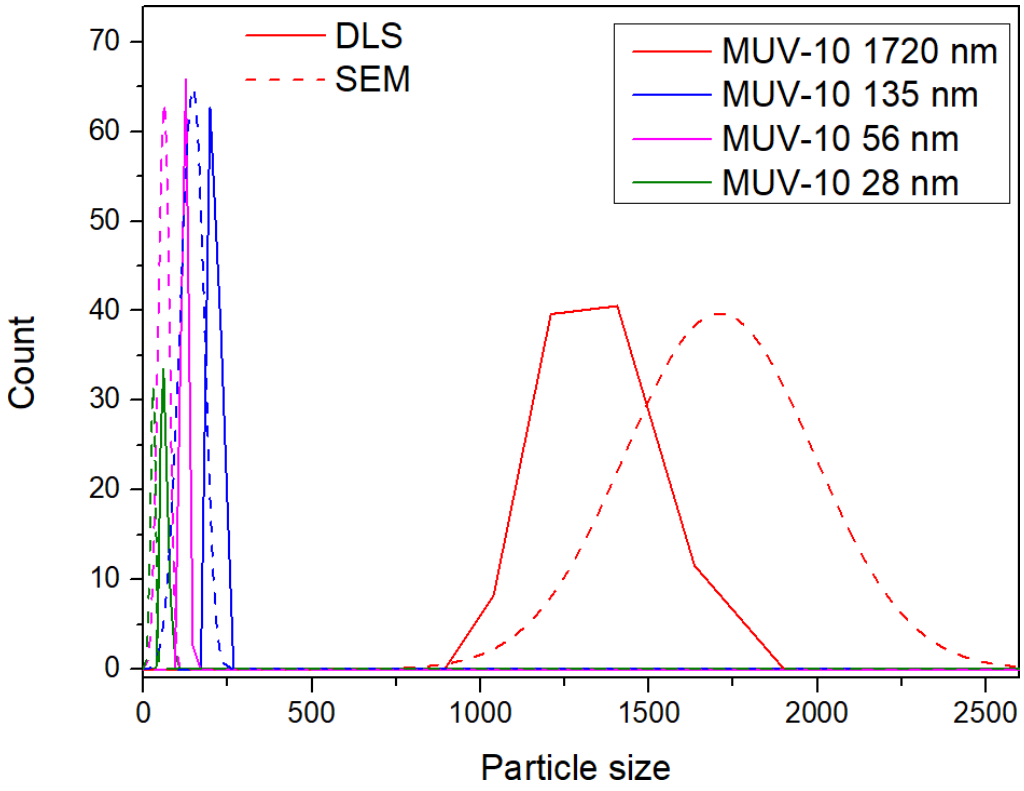


**Figure S13:** DLS measurements in PBS 10X compared with the gaussian distribution of the particle sizes determined by SEM.

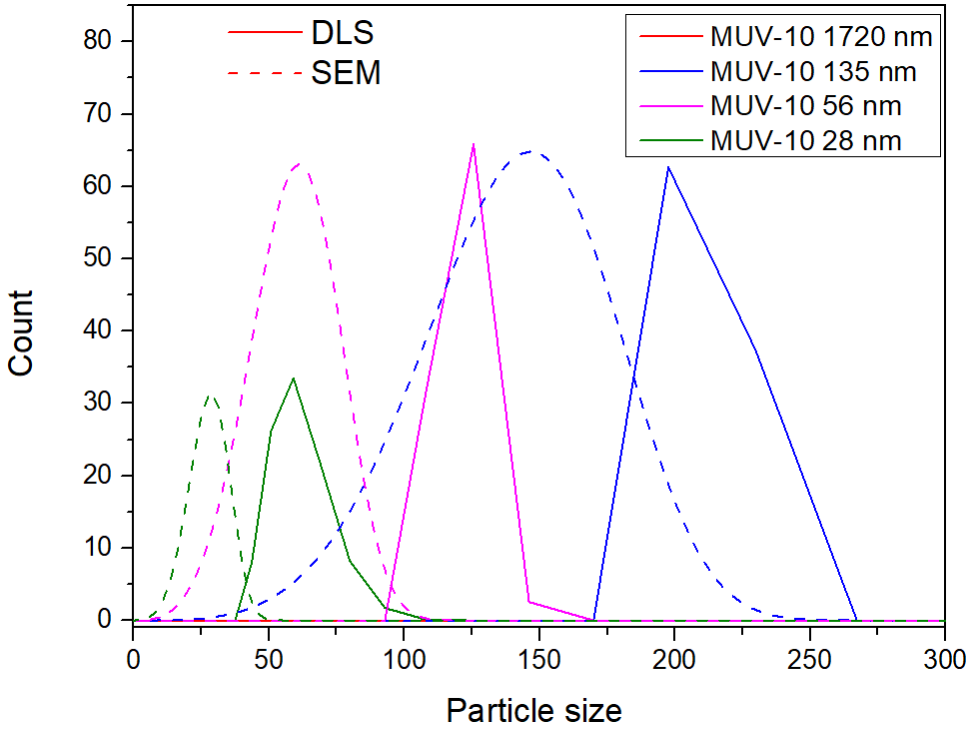


**Figure S14:** DLS measurements in PBS 10X compared with the gausian distribution of the particle sizes determined by SEM, showing minor aggregation of the MOFs.

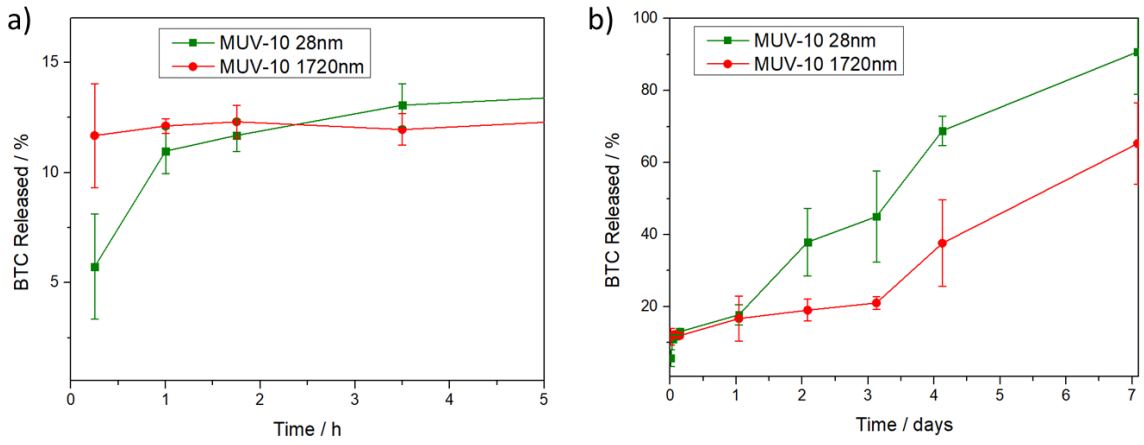


**Figure S15:** Degradation profiles in PBS 10X of the biggest and smallest particle size for three independent experiments performed in different days.

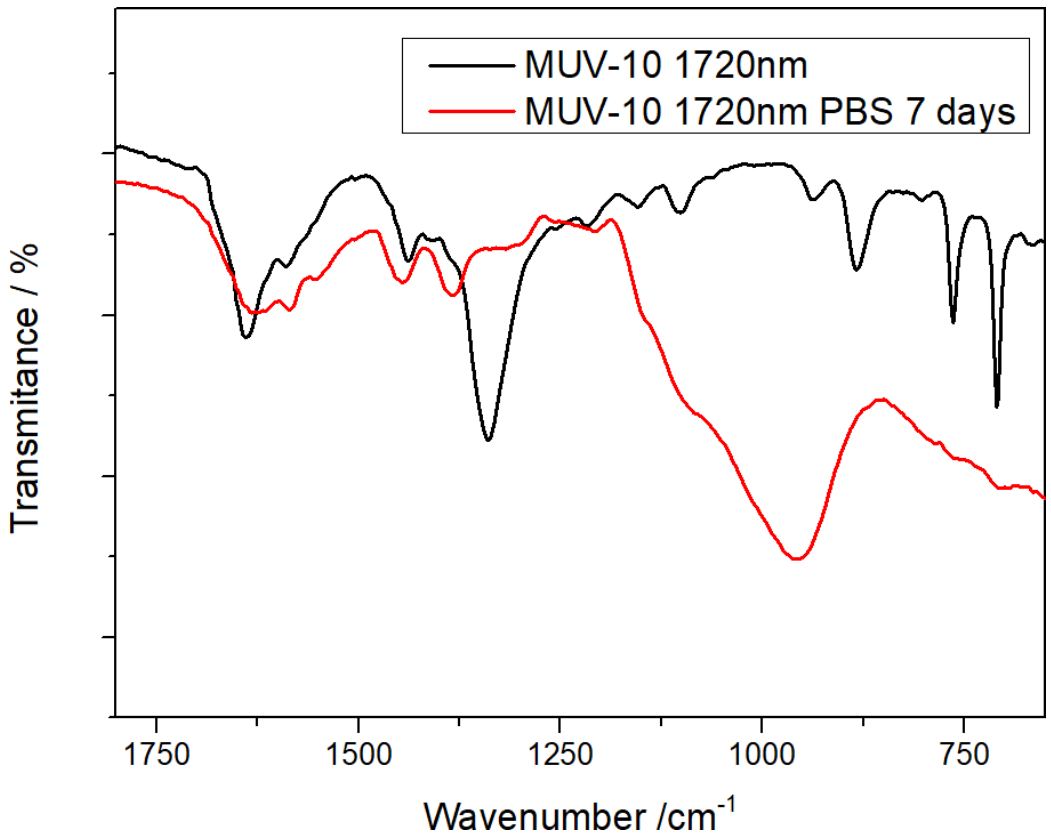


**Figure S16:** FT-IR profiles of MUV-10 1720 nm before and after phosphate-induced degradation, showing the attachment of phosphates (broad band at ca. 1000 $cm^{-1}$) and the degradation of the MOF.

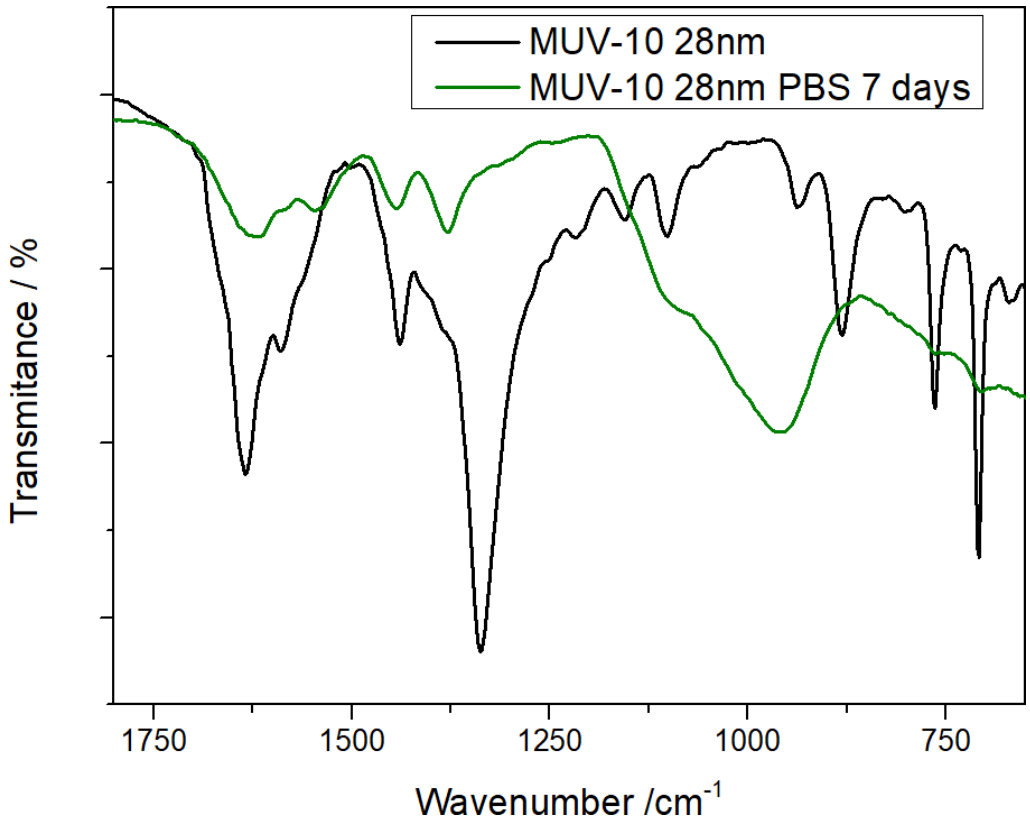


**Figure S17:** FT-IR profiles of MUV-10 28nm before and after phosphate-induced degradation, showing the attachment of phosphates (broad band at ca. 1000 $cm^{-1}$) and the degradation of the MOF.

## S.5. Characterisation of Calcein loaded MOFs

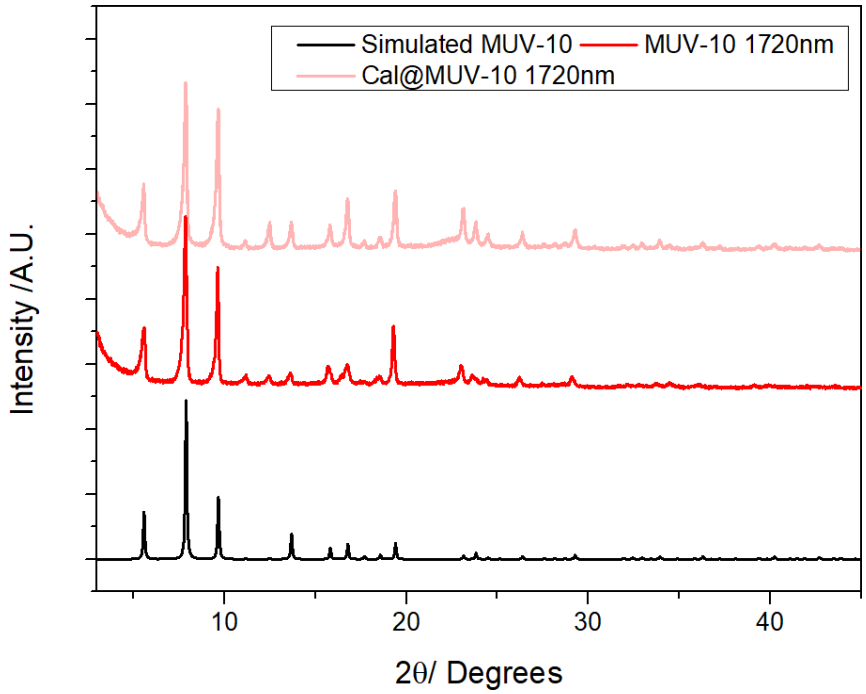


**Figure S18:** PXRD patterns of empty and calcein-loaded MUV-10 1720nm, showing structural integrity.

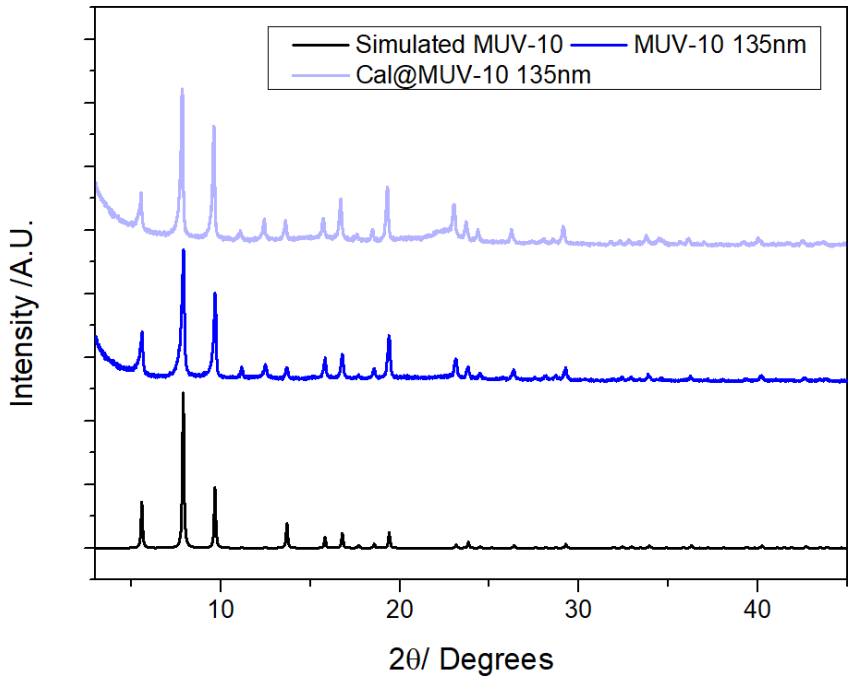


**Figure S19:** PXRD patterns of empty and calcein-loaded MUV-10 135nm, showing structural integrity.

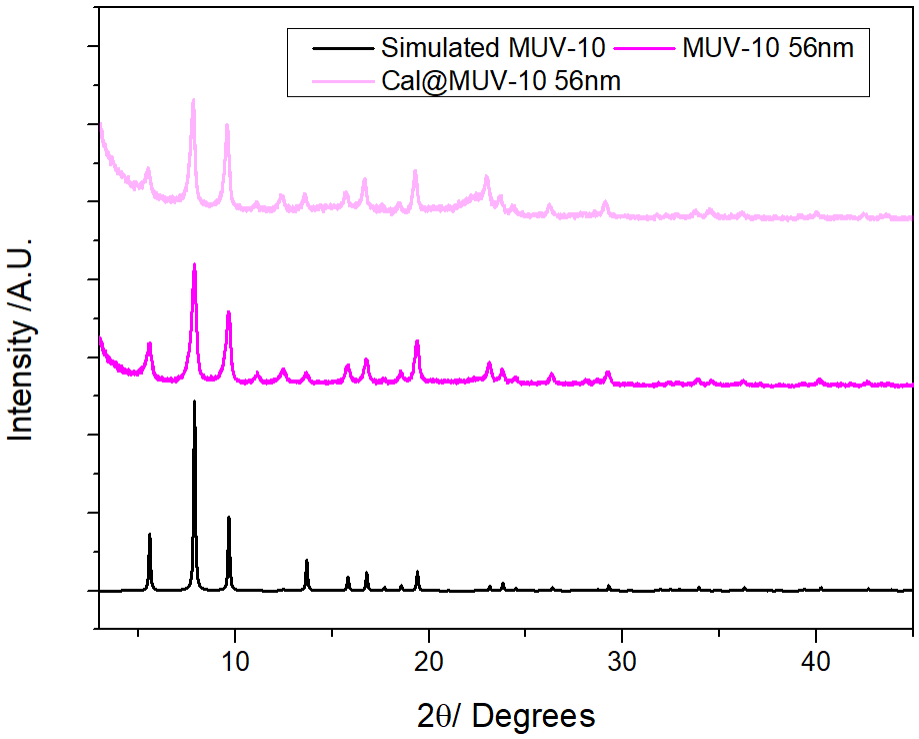


**Figure S20:** PXRD patterns of empty and calcein-loaded MUV-10 56nm, showing structural integrity.

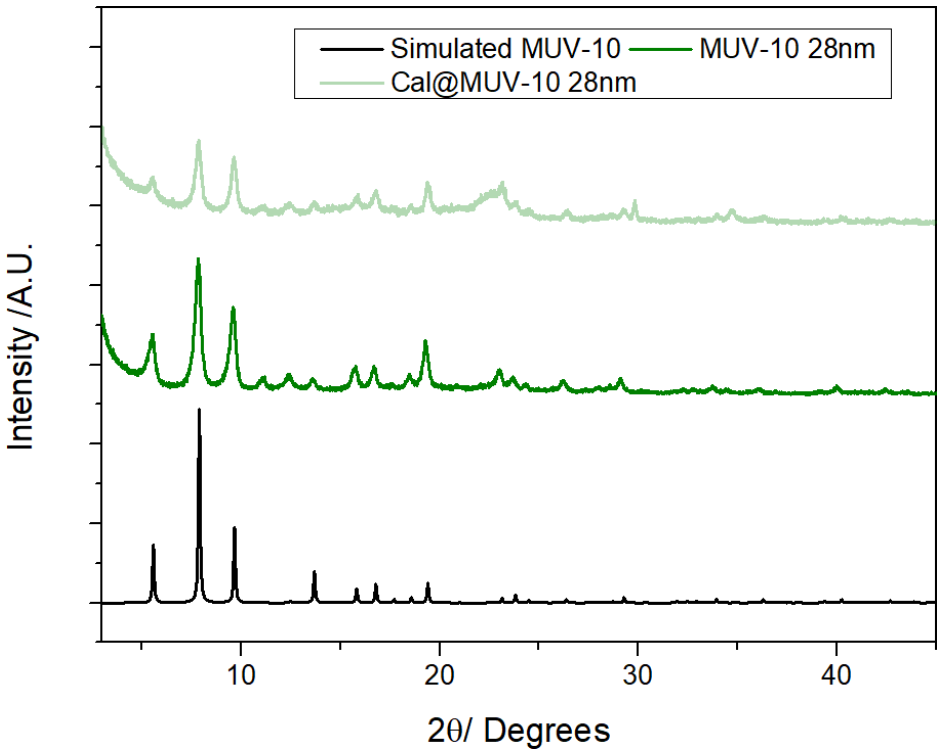


**Figure S21:** PXRD patterns of empty and calcein-loaded MUV-10 28nm, showing structural integrity.

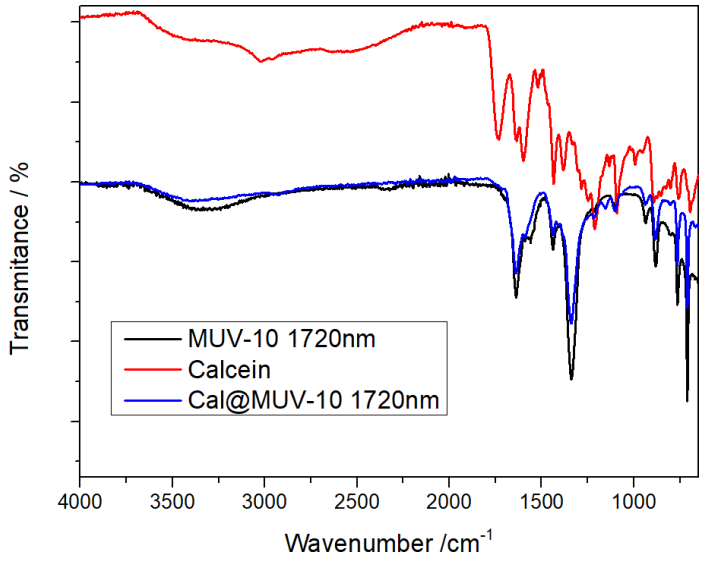


**Figure S22:**FT-IR profiles of calcein-loaded MUV-10 1720nm, compared to free calcein and empty MUV-10 1720 nm, showing that phase pure MUV-10 with the absence of free calcein, due to its attachment to the metals through its carboxylate units.

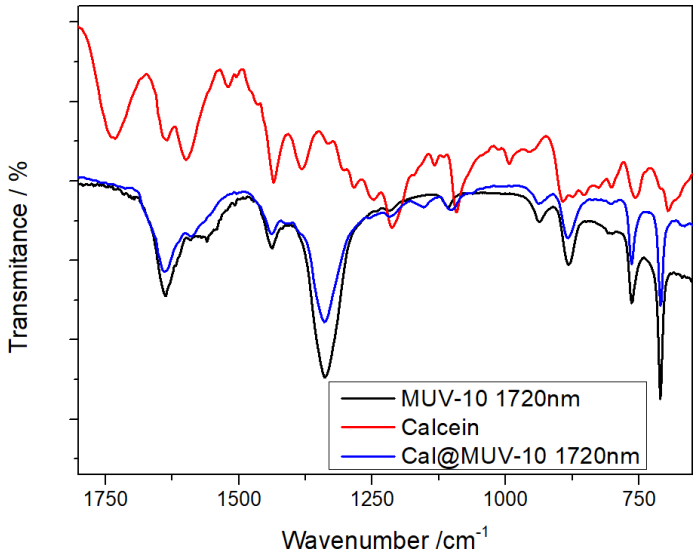


**Figure S23:**Amplification of FT-IR profiles of calcein-loaded MUV-10 1720nm, compared to free calcein and empty MUV-10 1720 nm, showing that phase pure MUV-10 with the absence of free calcein, due to its attachment to the metals through its carboxylate units, showing changes in the metal vibration bands and calcein characteristic signals, although the vast majority are masked by the MOF signals.

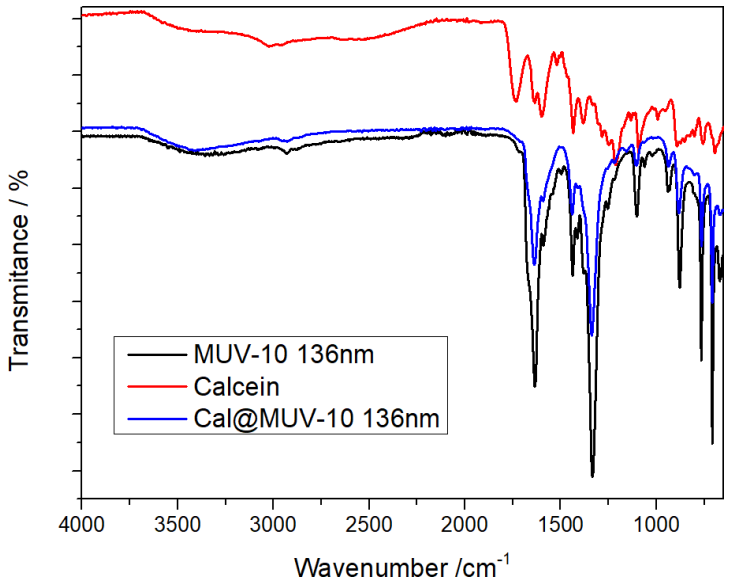


**Figure S24:**FT-IR profiles of calcein-loaded MUV-10 135nm, compared to free calcein and empty MUV-10 135 nm, showing that phase pure MUV-10 with the absence of free calcein, due to its attachment to the metals through its carboxylate units.

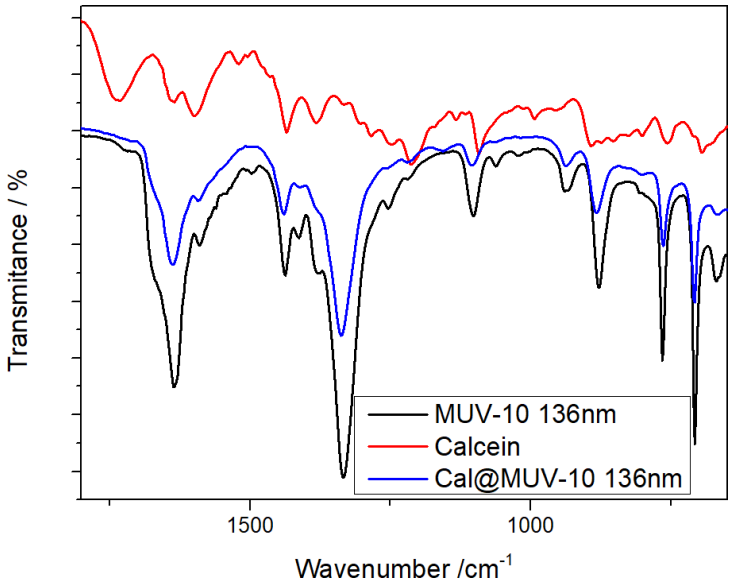


**Figure S25:**Amplification of FT-IR profiles of calcein-loaded MUV-10 135nm, compared to free calcein and empty MUV-10 135 nm, showing that phase pure MUV-10 with the absence of free calcein, due to its attachment to the metals through its carboxylate units, showing changes in the metal vibration bands and calcein characteristic signals, although the vast majority are masked by the MOF signals.

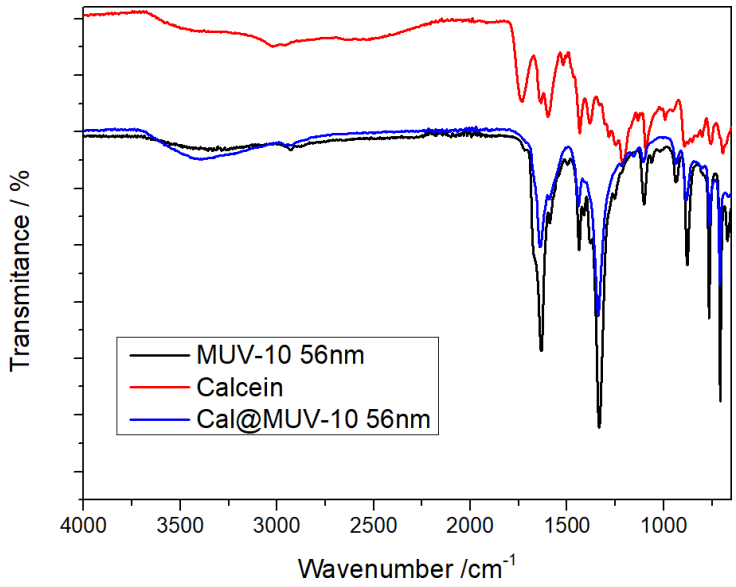


**Figure S26:**FT-IR profiles of calcein-loaded MUV-10 135nm, compared to free calcein and empty MUV-10 135 nm, showing that phase pure MUV-10 with the absence of free calcein, due to its attachment to the metals through its carboxylate units.

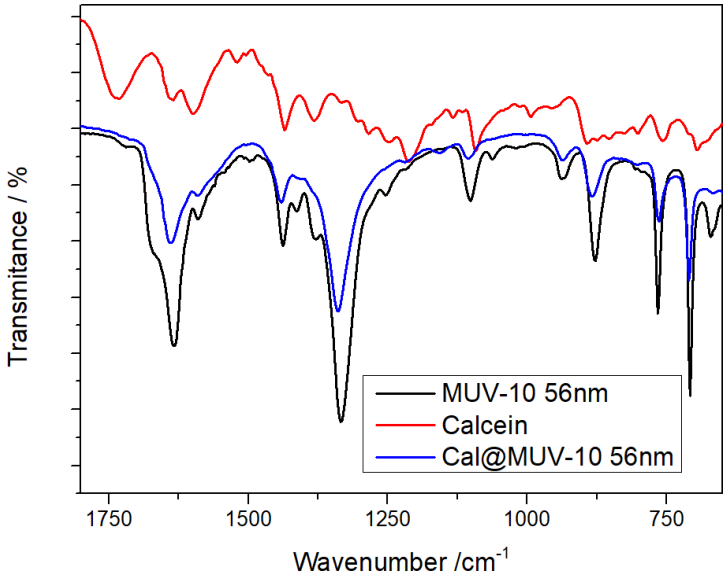


**Figure S27:**Amplification of FT-IR profiles of calcein-loaded MUV-10 56nm, compared to free calcein and empty MUV-10 56 nm, showing that phase pure MUV-10 with the absence of free calcein, due to its attachment to the metals through its carboxylate units, showing changes in the metal vibration bands and calcein characteristic signals, although the vast majority are masked by the MOF signals.

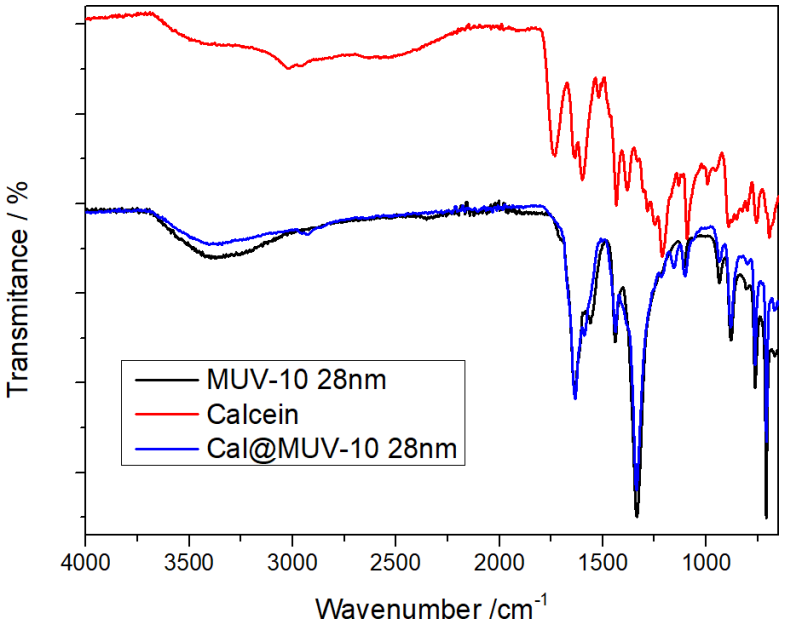


**Figure S28:**FT-IR profiles of calcein-loaded MUV-10 28nm, compared to free calcein and empty MUV-10 28 nm, showing that phase pure MUV-10 with the absence of free calcein, due to its attachment to the metals through its carboxylate units.

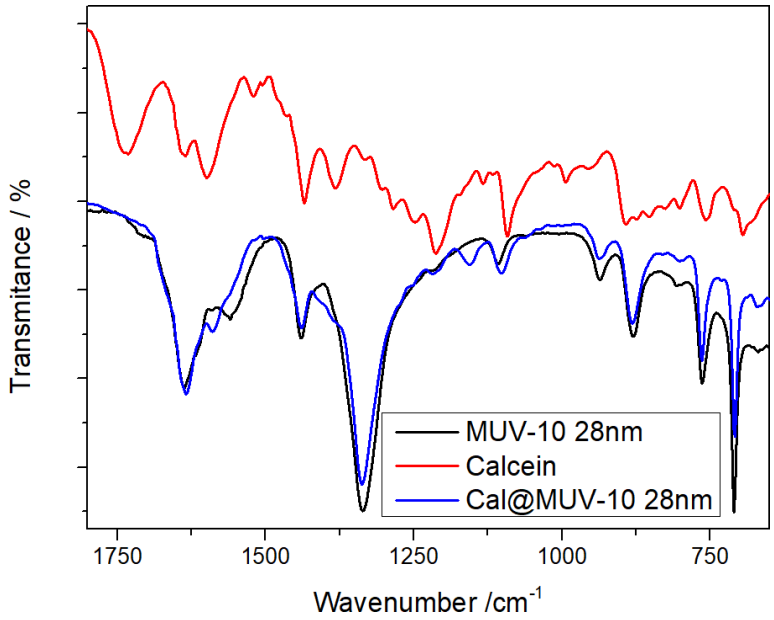


**Figure S29:**Amplification of FT-IR profiles of calcein-loaded MUV-10 28nm, compared to free calcein and empty MUV-10 28 nm, showing that phase pure MUV-10 with the absence of free calcein, due to its attachment to the metals through its carboxylate units, showing changes in the metal vibration bands and calcein characteristic signals, although the vast majority are masked by the MOF signals.

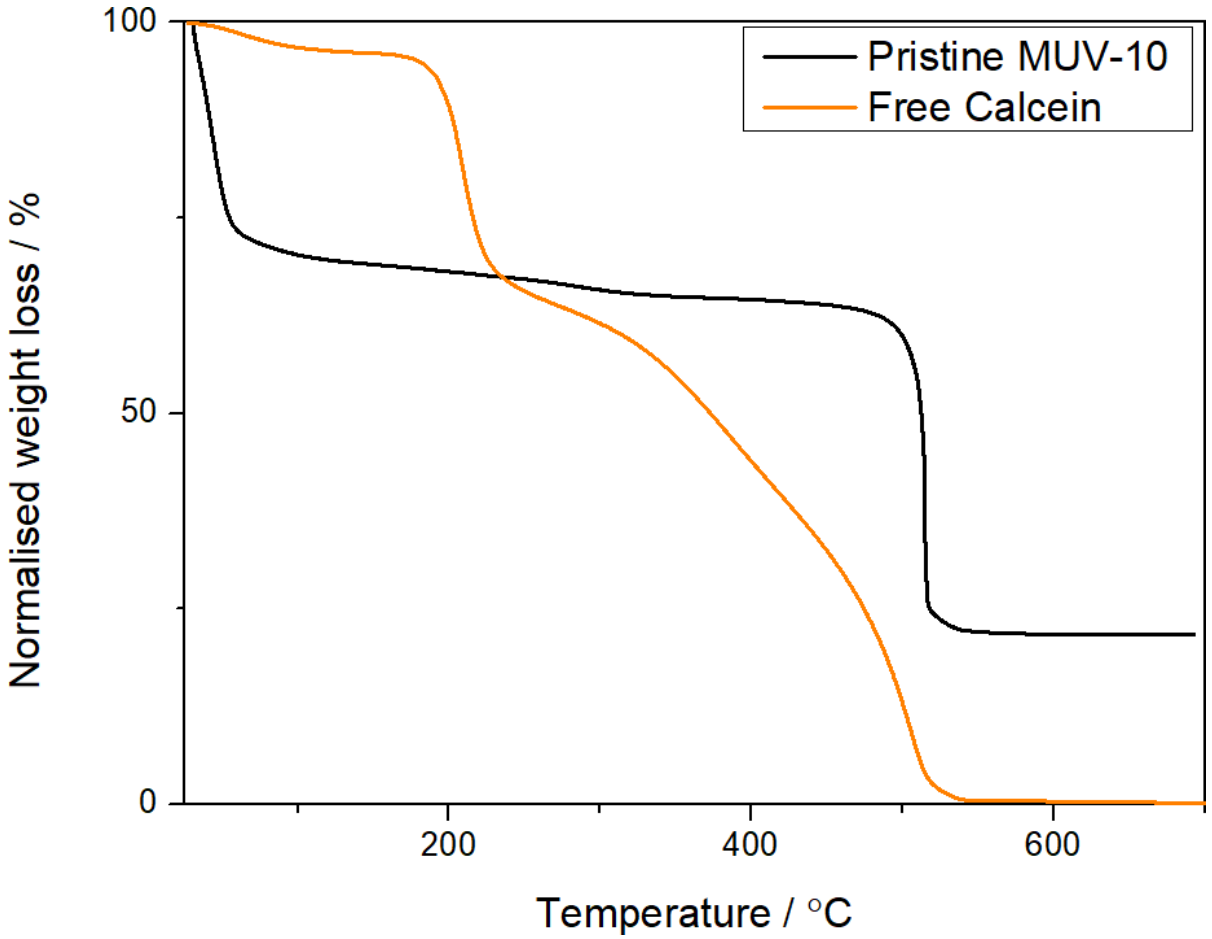


**Figure S30:** TGA profiles of pristine MUV-10 and Free calcein, showing the gradual decomposition profile of calcein that overlaps with the decomposition events of the MOF.

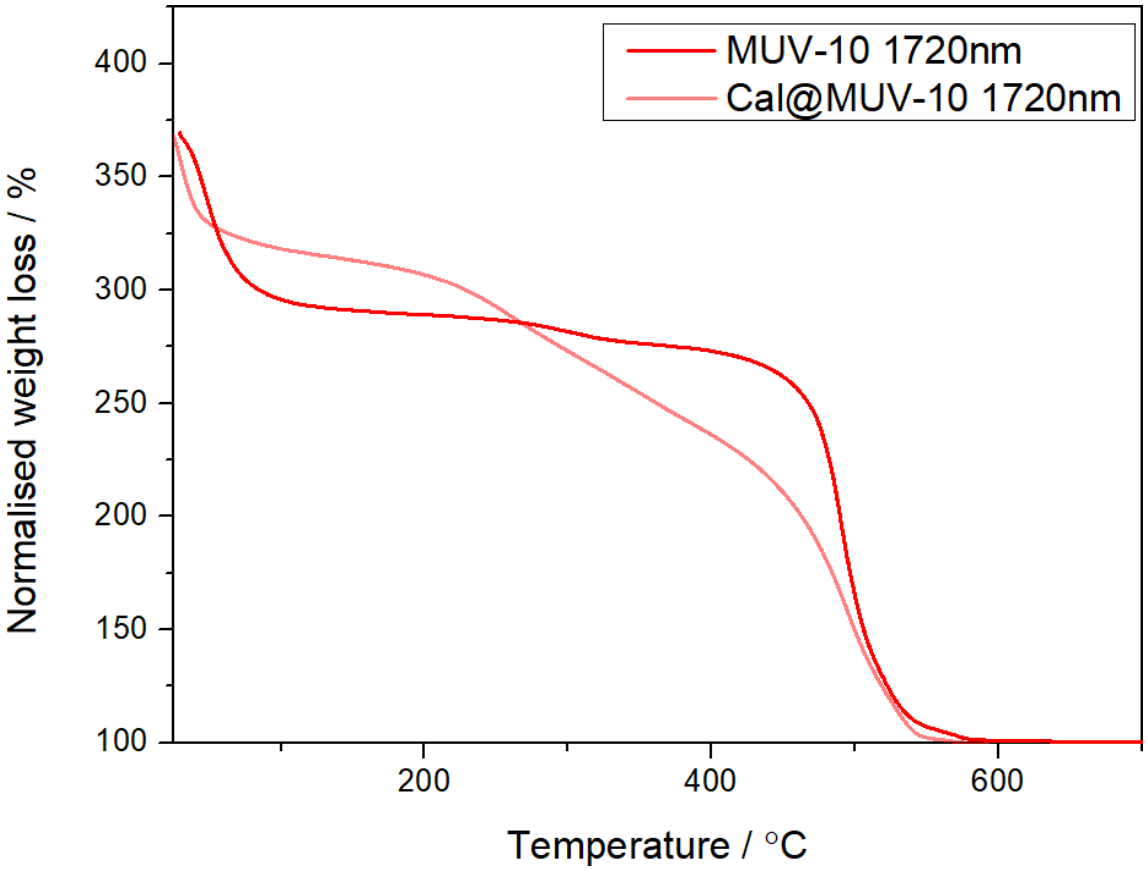


**Figure S31:** TGA profiles of empty and calcein-loaded MUV-10 1720 nm, showing an increase in the organic content as a consequence of calcein-loading, alongside with more gradual decomposition profile and reduction linker decomposition step (starting at ca. 450 °C) that indicates calcein attachment through a surface ligand step process.

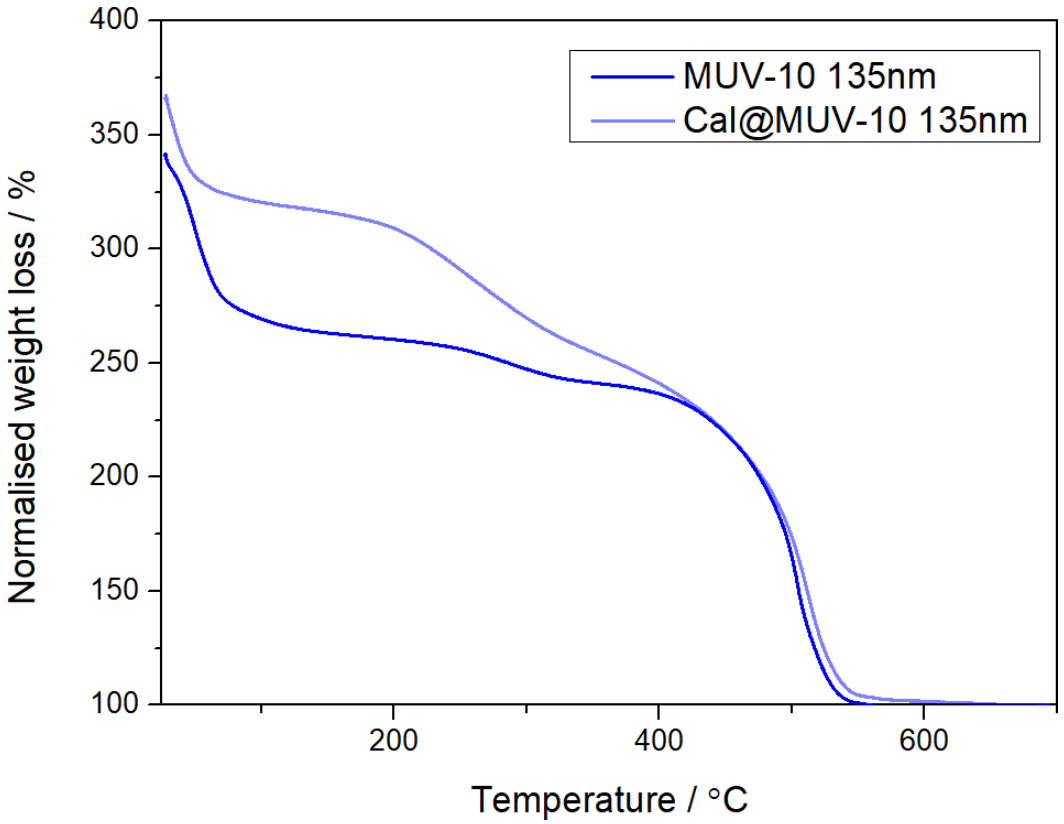


**Figure S32:** TGA profiles of empty and calcein-loaded MUV-10 135 nm, showing an increase in the organic content as a consequence of calcein-loading, alongside with more gradual decomposition profile and a maintained linker decomposition step (starting at ca. 450 °C) that indicates calcein attachment through a surface ligand step process, given that calcein loading overlaps with the linker decomposition.

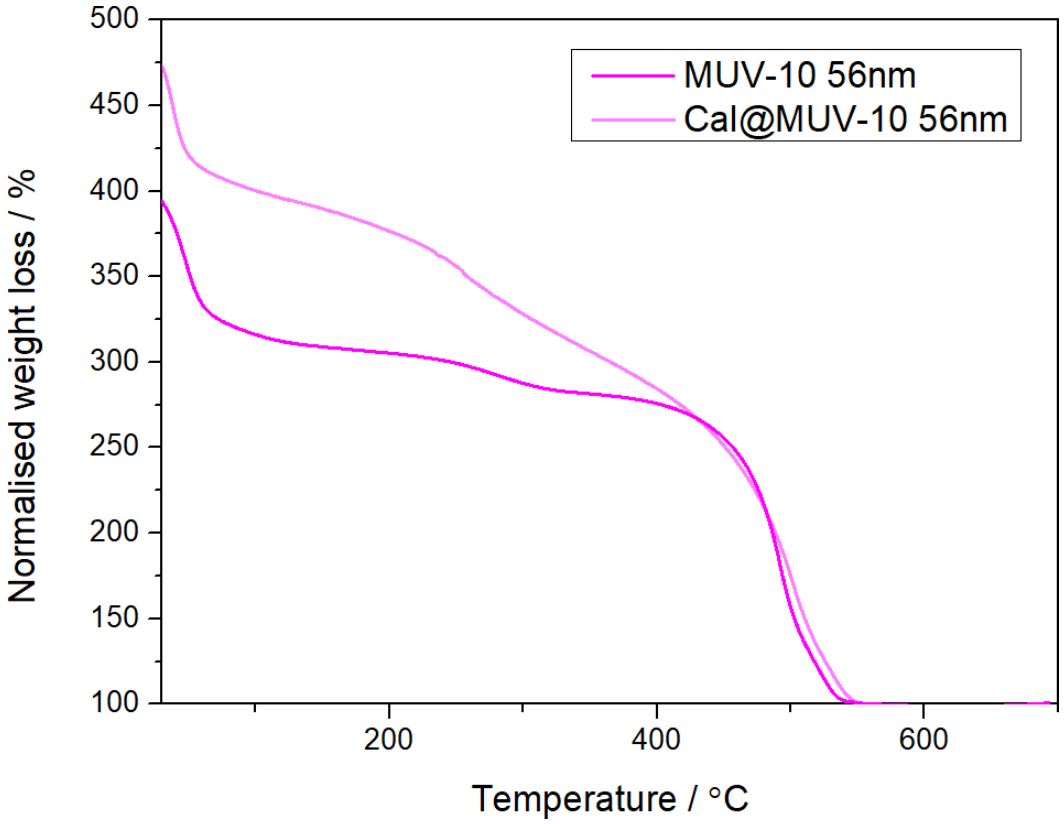


**Figure S33:** TGA profiles of empty and calcein-loaded MUV-1056 nm, showing an increase in the organic content as a consequence of calcein-loading, alongside with more gradual decomposition profile and a maintained linker decomposition step (starting at ca. 450 °C) that indicates calcein attachment through a surface ligand step process, given that calcein loading overlaps with the linker decomposition.

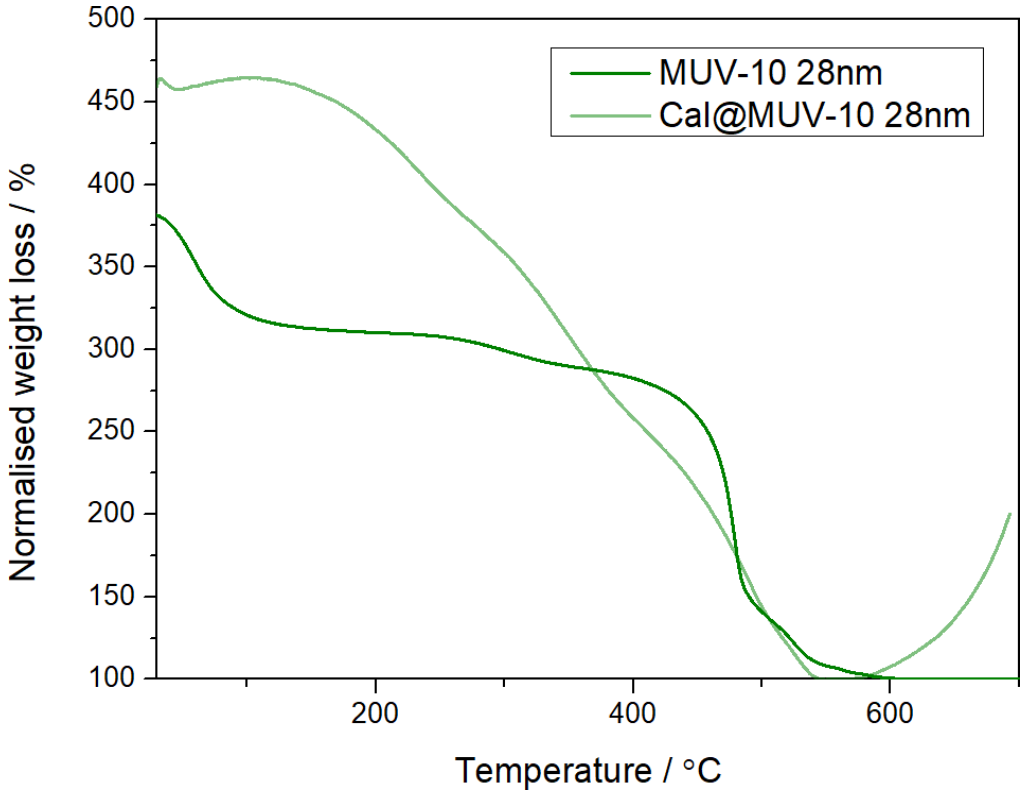


**Figure S34:** TGA profiles of empty and calcein-loaded MUV-10 28 nm, showing an increase in the organic content as a consequence of calcein-loading, alongside with more gradual decomposition profile and a reduced linker decomposition step (starting at ca. 450 °C) that indicates calcein attachment through a surface ligand step process, further supported by the oxidation of the sample, indicative of the low presence of linkers.

As the molecular mass of the MOF is known throughout the previous thermal analysis if assuming structural integrity, and the molecular mass of calcein is also known TGA[2] can be applied to calculate the calcein-loading as follows:

Since,

$$S\%MOF = 1 - S\%Composite; \quad MS\%Composite = 1 - S\%MOF$$

Then,

$$R_{exp} = \left(\frac{(M_w[MOF] * S\%MOF) + (M_w[Calcein] * (1 - S\%MOF))}{M_w\,[TiCaO_3] * S\%MOF}\right)$$

Rearrangement of the equation,

$$R_{exp} * M_w\,[TiCaO_3] - M_w[MOF] = \left(\frac{(M_w[Calcein] * (1 - S\%MOF))}{S\%MOF}\right)$$

$$R_{exp} * M_w\,[TiCaO_3] - Mw\,[MOF] + M_w[Calcein] = \left(\frac{(M_w[Calcein]}{S\%MOF}\right)$$

Then,

$$S\%MOF = \left(\frac{(M_w[Calcein]}{R_{exp} * M_w\,[TiCaO_3] - M_w[MOF] + M_w[Calcein]}\right)$$

**Table S6:** Tabulated Calcein Loading of MUV-10 with different techniques, suggesting together with FT-IR showing no free carboxylate calcein vibration bands, that through the calcein loading process surface ligands are exchanged by calcein, and thus the loading determined by UV-VIS is higher than the loading determined by TGA. In fact the loading % increases with the reduction of particle size, indicating that a significant amount of the calcein is attached to the MOFs surface. Additionally, the differences between the characterization methods are more significant with the reduction of the particle size. This concludes that TGA is not a good method to determine calcein loading given that structural integrity is not maintained due to the ligand exchange process.

| **Samples** | **Calcein wt% UV-Vis** | **Calcein wt % TGA** |
|---|---|---|
| **1720nm** | 9.51 | 6.35 |
| **135nm** | 14.97 | 11.35 |
| **56nm** | 26.28 | 21.18 |
| **28nm** | 33.62 | 25.41 |

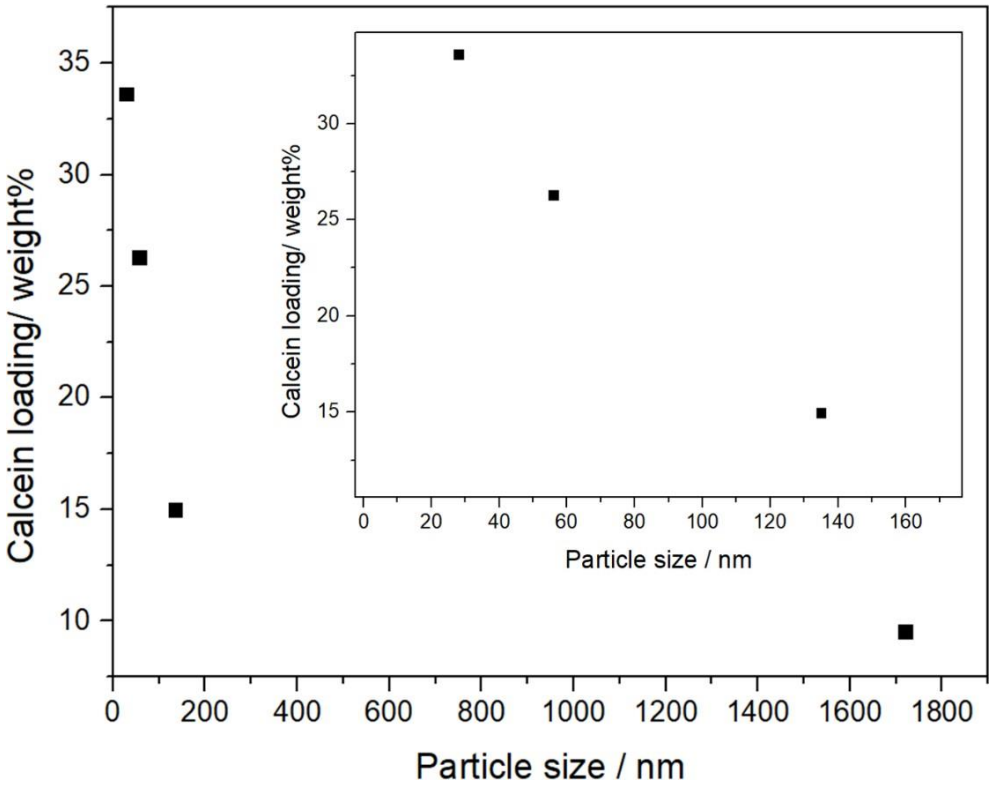


**Figure S35:**Relation between the particle size and calcein loading determided by UV-Vis.

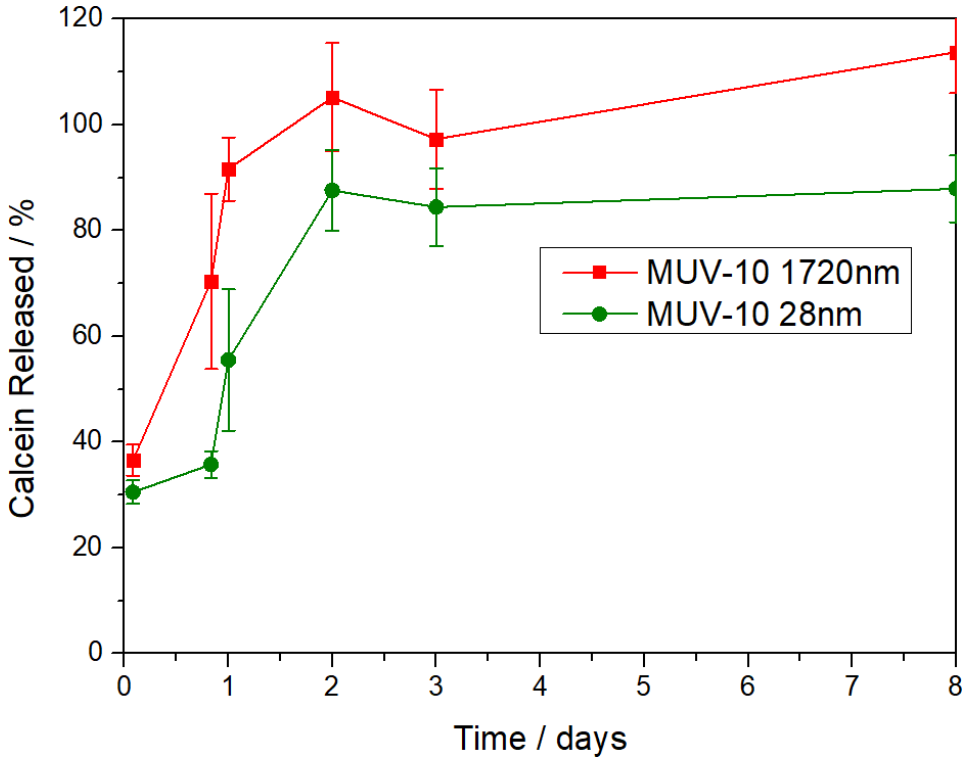


**Figure S36:**Calcein release profiles in PBS 10X of the biggest and smallest particle size for three independent experiments performed in different days.

## S.6. Cell Internalisation

Cell internalisation assays were carried out as described in **Section S3.1.**

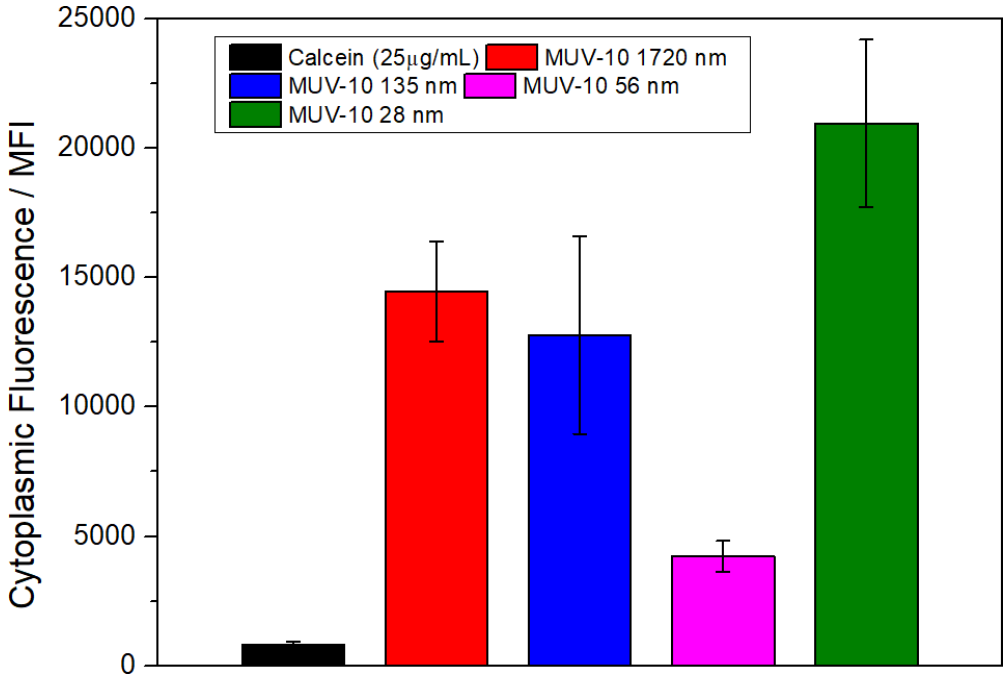


**Figure S37:**Macrophage J744 internalisation of calcein-loaded MOFs (250 µgmL-1) compared to free calcein.

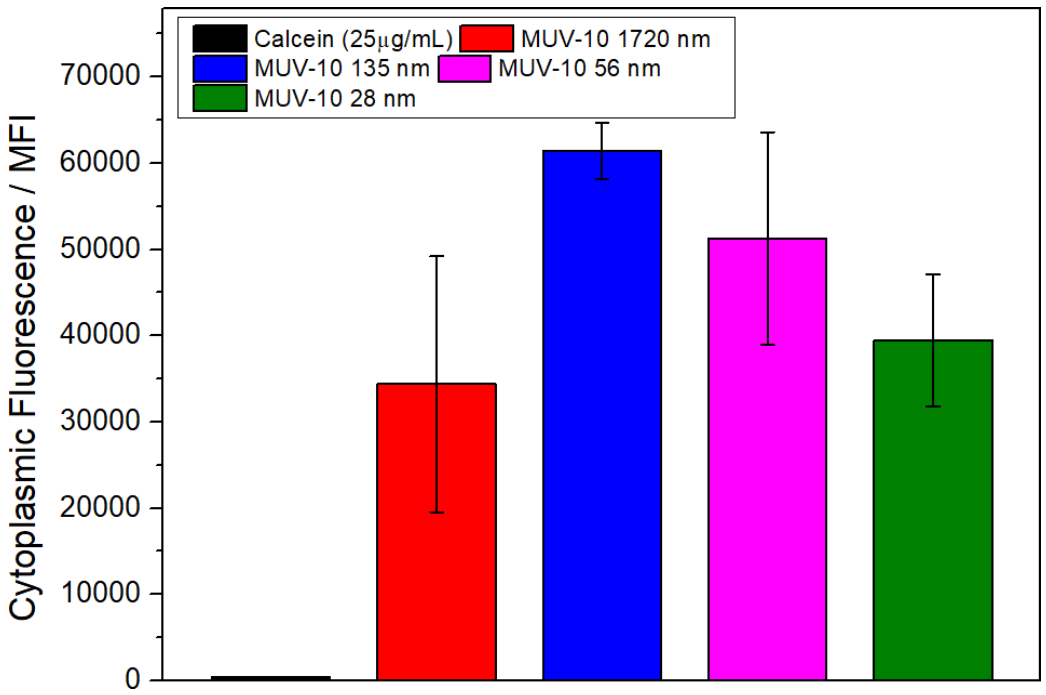


**Figure S38:**PBM cells internalisation of calcein-loaded MOFs (250 µgmL-1) compared to free calcein.

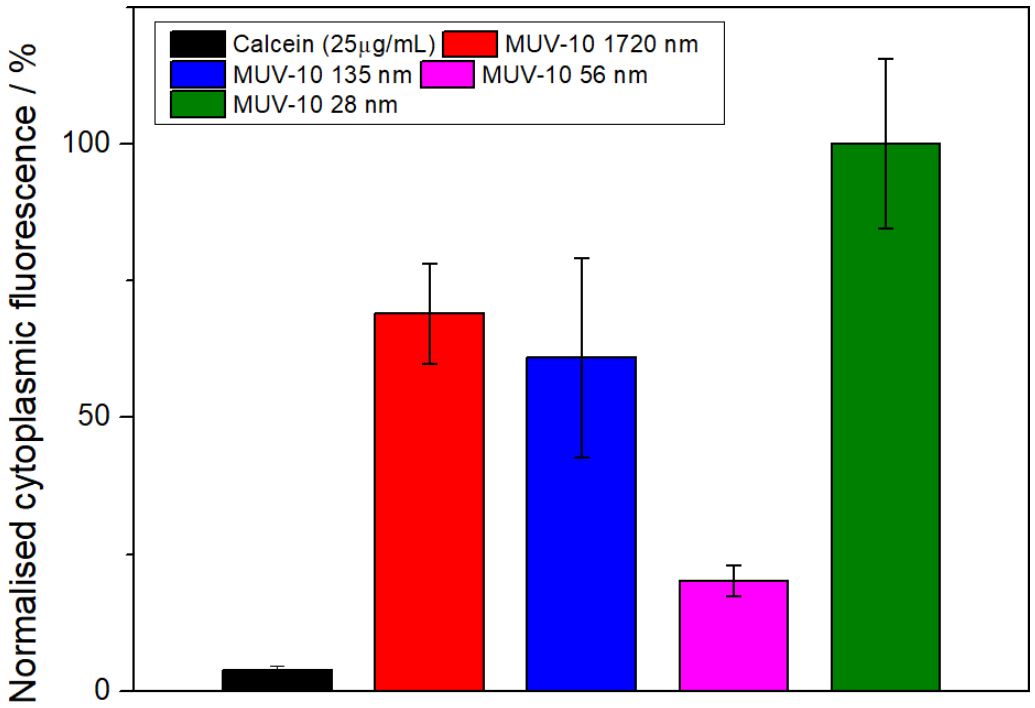


**Figure S39:**Normalised macrophage J744 internalisation of calcein-loaded MOFs (250 µgmL-1) compared to free calcein. Normalisation performed using the maximum IMF as the 100%.

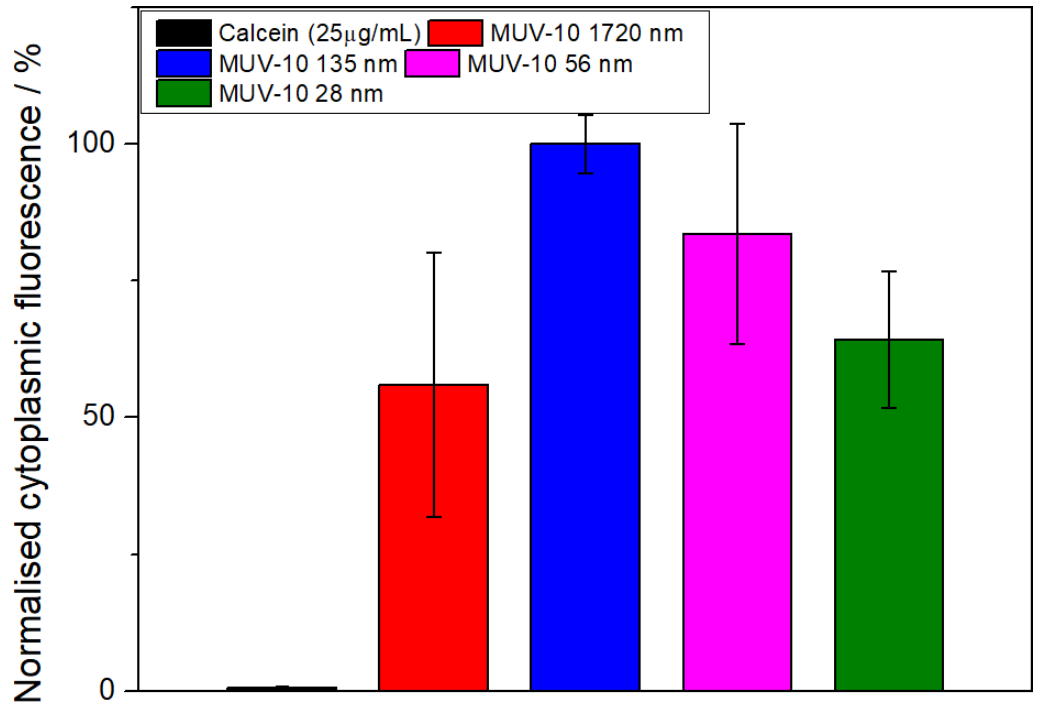


**Figure S40:**Normalised PBM cells internalisation of calcein-loaded MOFs (250 µgmL-1) compared to free calcein. Normalisation performed using the maximum IMF as the 100%.

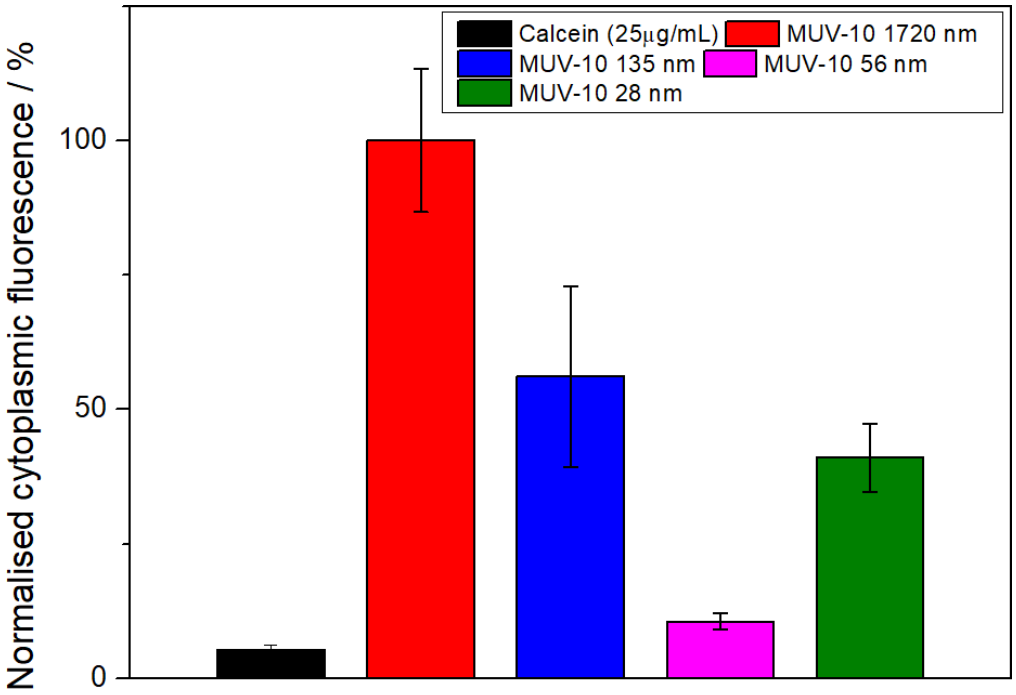


**Figure S41:**Normalised macrophage J744 internalisation of calcein-loaded MOFs (250 µgmL-1) compared to free calcein. Normalisation performed using the IMF divided by the maximum calcein delivered dose as the 100%.

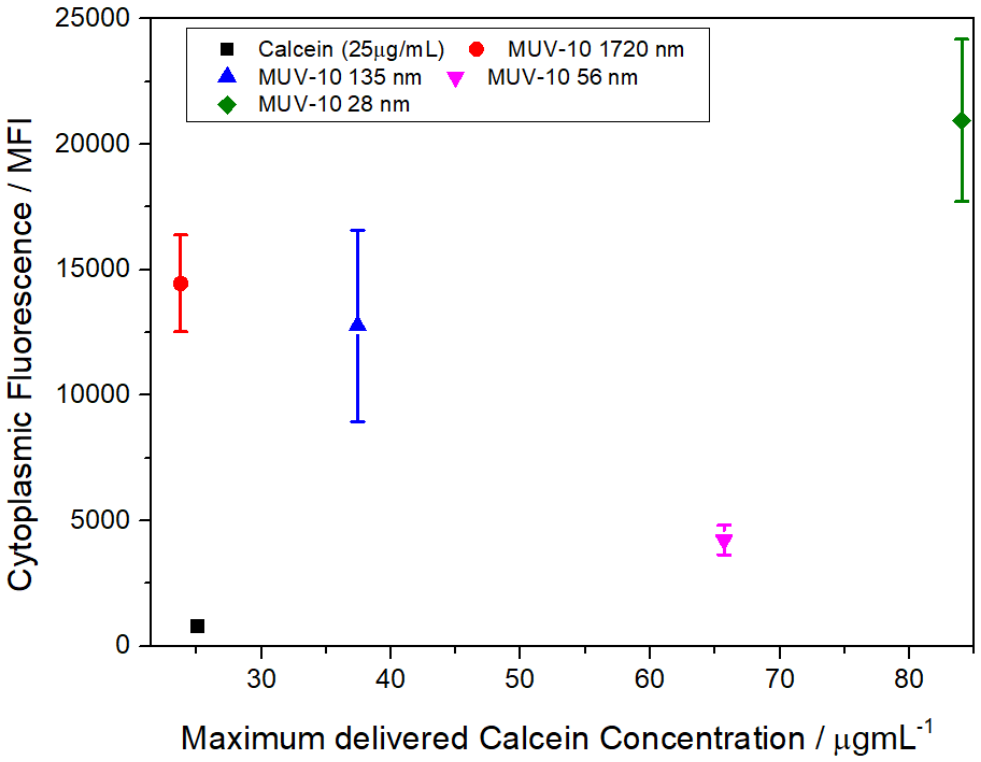


**Figure S42:**Macrophage J744 internalisation of calcein-loaded MOFs (250 µgmL-1) compared to free calcein, represented as a function of the maximum calcein delivered dose.

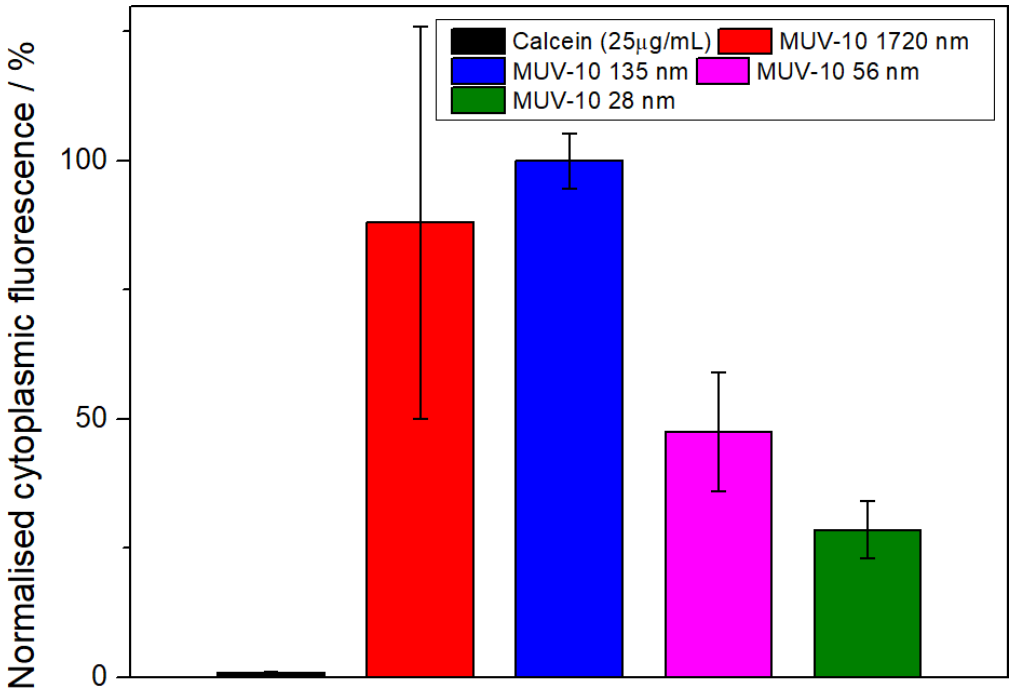


**Figure S43:**Normalised PBM cell internalisation of calcein-loaded MOFs (250 µgmL-1) compared to free calcein. Normalisation performed using the IMF divided by the maximum calcein delivered dose as the 100%.

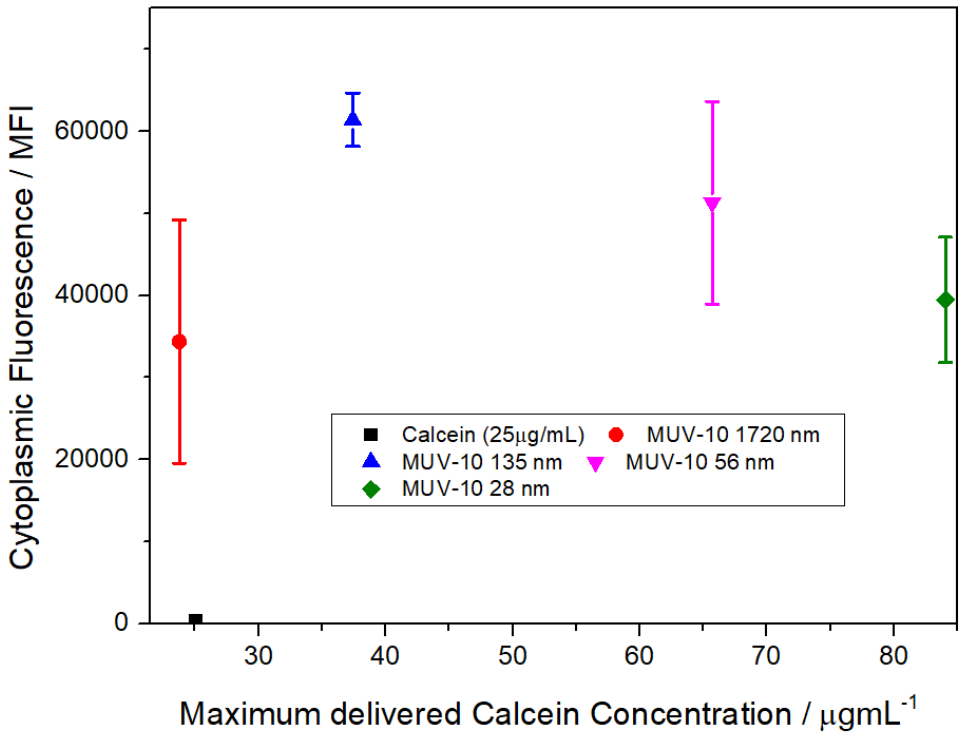


**Figure S44:**PBM cells internalisation of calcein-loaded MOFs (250 µgmL-1) compared to free calcein, represented as a function of the maximum calcein delivered dose.

## S.7. Cytotoxicity experiments

### S.7.1 MTT

MTS assays were carried out as described **in Section S3.2.** The represented values are the average of 3 different experiment, each of them with n=3.

### S.7.1.A MTT essays with Macrophages J744

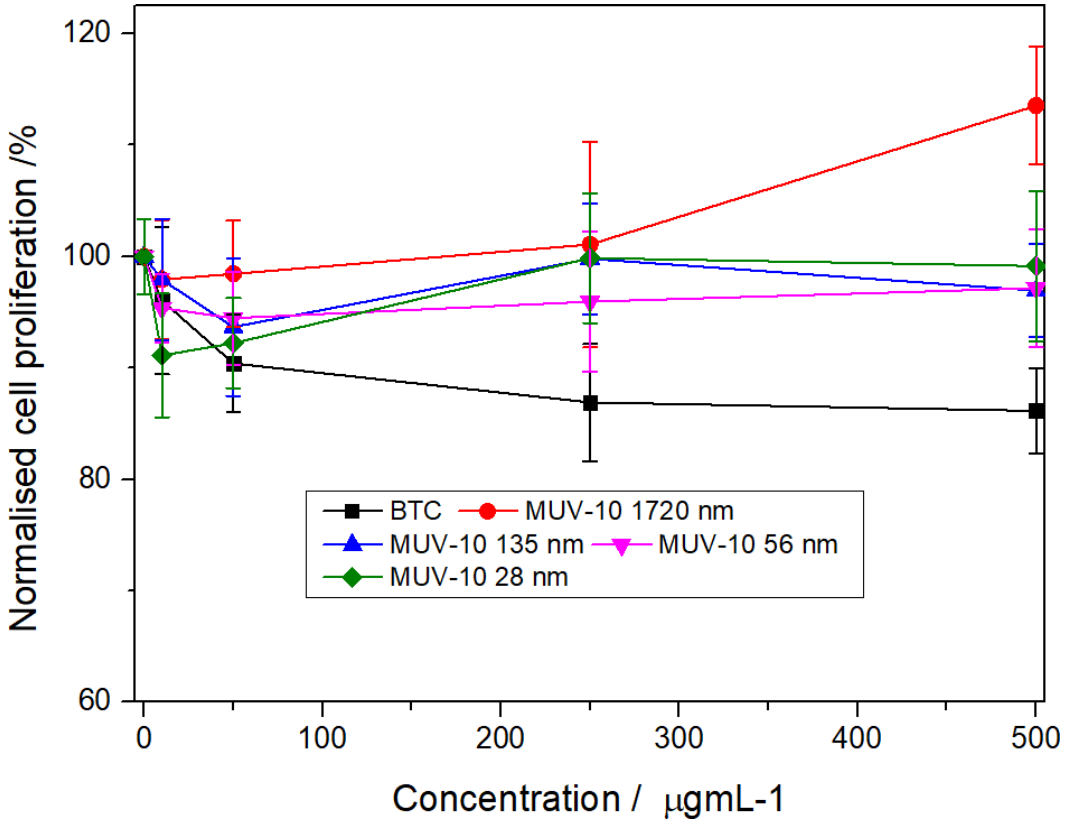


**Figure S45:** Cytotoxicity of MUV-10 samples measured by MTT assay towards J774 macrophage cells after 24 hours of incubation. (3 independent experiments performed in different days, each of them with n=3).

**Table S7:** Macrophage cells viability data upon incubation with BTC during 24 hours for three different experiments performed on different days, each of them with n=3

| Conc. (µg/mL) | Av 1 (%) | Error 1(%) | Av 2(%) | Error 2(%) | Av 3 (%) | Error 3 (%) |
|---|---|---|---|---|---|---|
| 0 | 100.00 | 1.42 | 100.00 | 4.02 | 100.00 | 4.65 |
| 10 | 99.21 | 9.85 | 94.31 | 4.09 | 94.61 | 5.90 |
| 50 | 98.02 | 5.48 | 86.62 | 3.37 | 86.60 | 4.24 |
| 250 | 87.75 | 7.30 | 89.02 | 5.38 | 83.94 | 3.07 |
| 500 | 85.49 | 3.78 | 90.63 | 2.71 | 82.31 | 5.09 |

**Table S8:** Macrophage cells viability data upon incubation with MUV-10 1720 nm during 24 hours for three different experiments performed on different days, each of them with n=3

| Conc. (µg/mL) | Av 1 (%) | Error 1(%) | Av 2(%) | Error 2(%) | Av 3 (%) | Error 3 (%) |
|---|---|---|---|---|---|---|
| 0 | 100.00 | 1.42 | 100.00 | 4.02 | 100.00 | 4.65 |
| 10 | 89.21 | 4.17 | 105.91 | 5.81 | 98.67 | 6.09 |
| 50 | 92.43 | 3.59 | 107.22 | 6.92 | 95.69 | 3.82 |
| 250 | 100.32 | 4.49 | 107.58 | 11.57 | 95.36 | 11.68 |
| 500 | 114.59 | 4.77 | 124.67 | 6.88 | 101.36 | 4.19 |

**Table S9:** Macrophage cells viability data upon incubation with MUV-10 135 nm during 24 hours for three different experiments performed on different days, each of them with n=3

| Conc. (µg/mL) | Av 1 (%) | Error 1(%) | Av 2(%) | Error 2(%) | Av 3 (%) | Error 3 (%) |
|---|---|---|---|---|---|---|
| 0 | 100.00 | 1.42 | 100.00 | 4.02 | 100.00 | 4.65 |
| 10 | 95.85 | 5.27 | 101.60 | 3.96 | 96.34 | 7.11 |
| 50 | 97.64 | 5.35 | 96.68 | 4.31 | 86.69 | 8.91 |
| 250 | 98.57 | 4.74 | 107.86 | 7.02 | 92.96 | 3.21 |
| 500 | 99.38 | 2.20 | 99.24 | 3.92 | 92.21 | 6.52 |

**Table S10:** Macrophage cells viability data upon incubation with MUV-10 56 nm during 24 hours for three different experiments performed on different days, each of them with n=3

| Conc. (µg/mL) | Av 1 (%) | Error 1(%) | Av 2(%) | Error 2(%) | Av 3 (%) | Error 3 (%) |
|---|---|---|---|---|---|---|
| 0 | 100.00 | 1.42 | 100.00 | 4.02 | 100.00 | 4.65 |
| 10 | 94.18 | 1.07 | 97.76 | 4.58 | 94.18 | 3.58 |
| 50 | 94.54 | 1.72 | 92.37 | 4.30 | 96.52 | 6.56 |
| 250 | 99.30 | 10.23 | 96.70 | 4.03 | 91.85 | 4.67 |
| 500 | 97.92 | 2.74 | 97.88 | 7.98 | 95.69 | 5.20 |

**Table S11:** Macrophage cells viability data upon incubation with MUV-10 28 nm during 24 hours for three different experiments performed on different days, each of them with n=3

| Conc. (µg/mL) | Av 1 (%) | Error 1(%) | Av 2(%) | Error 2(%) | Av 3 (%) | Error 3 (%) |
|---|---|---|---|---|---|---|
| 0 | 100.00 | 4.02 | 100.00 | 4.65 | 100.00 | 1.42 |
| 10 | 97.81 | 4.04 | 90.66 | 5.77 | 84.93 | 6.90 |
| 50 | 100.09 | 4.84 | 89.50 | 3.95 | 87.07 | 3.32 |
| 250 | 104.79 | 6.95 | 103.43 | 5.19 | 91.41 | 5.38 |
| 500 | 108.15 | 10.32 | 93.20 | 3.39 | 96.08 | 6.52 |

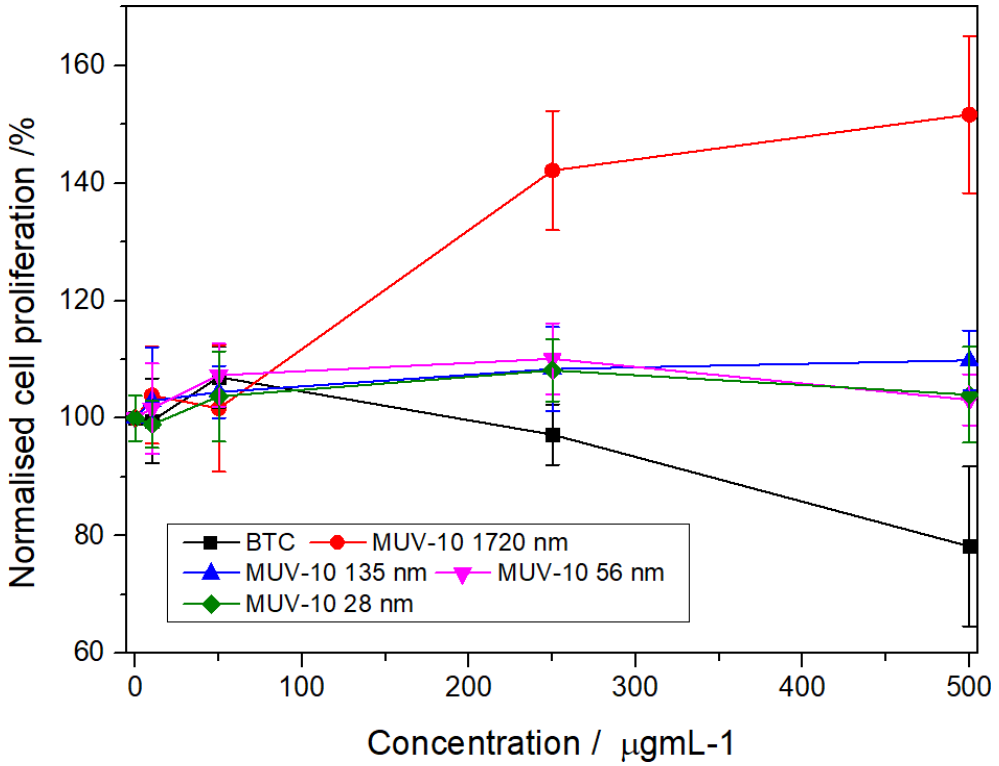


**Figure S46:** Cytotoxicity of MUV-10 samples measured by MTT assay towards J774 macrophage cells after 72 hours of incubation. (3 independent experiments performed in different days, each of them with n=3).

**Table S12:** Macrophage cells viability data upon incubation with BTC during 72 hours for three different experiments performed on different days, each of them with n=3

| Conc. (μg/mL) | Av 1 (%) | Error 1(%) | Av 2(%) | Error 2(%) | Av 3 (%) | Error 3 (%) |
|---|---|---|---|---|---|---|
| 0 | 100.00 | 5.86 | 100.00 | 1.27 | 100.00 | 4.36 |
| 10 | 113.99 | 11.43 | 91.45 | 2.01 | 93.29 | 8.09 |
| 50 | 121.62 | 8.52 | 99.83 | 2.33 | 99.58 | 4.72 |
| 250 | 107.08 | 4.78 | 89.39 | 2.61 | 95.18 | 7.98 |
| 500 | 95.34 | 13.25 | 73.19 | 10.50 | 66.13 | 17.01 |

**Table S13:** Macrophage cells viability data upon incubation with MUV-10 1720 nm during 72 hours for three different experiments performed on different days, each of them with n=3

| Conc. (µg/mL) | Av 1 (%) | Error 1(%) | Av 2(%) | Error 2(%) | Av 3 (%) | Error 3 (%) |
|---|---|---|---|---|---|---|
| 0 | 100.00 | 5.86 | 100.00 | 1.27 | 100.00 | 4.36 |
| 10 | 119.52 | 11.43 | 89.85 | 7.14 | 102.34 | 6.11 |
| 50 | 128.94 | 10.90 | 80.57 | 16.05 | 95.55 | 5.45 |
| 250 | 162.64 | 14.46 | 108.53 | 3.03 | 155.32 | 12.98 |
| 500 | 185.40 | 29.30 | 120.45 | 5.24 | 149.10 | 5.57 |

**Table S14:** Macrophage cells viability data upon incubation with MUV-10 156 nm during 72 hours for three different experiments performed on different days, each of them with n=3

| Conc. (µg/mL) | Av 1 (%) | Error 1(%) | Av 2(%) | Error 2(%) | Av 3 (%) | Error 3 (%) |
|---|---|---|---|---|---|---|
| 0 | 100.00 | 5.86 | 100.00 | 1.27 | 100.00 | 4.36 |
| 10 | 116.94 | 17.17 | 92.93 | 3.11 | 99.07 | 6.98 |
| 50 | 121.95 | 5.82 | 91.36 | 2.67 | 100.07 | 4.79 |
| 250 | 122.47 | 5.28 | 92.26 | 7.42 | 110.37 | 8.76 |
| 500 | 131.14 | 8.79 | 97.45 | 1.85 | 101.00 | 4.57 |

**Table S15:** Macrophage cells viability data upon incubation with MUV-10 35 nm during 72 hours for three different experiments performed on different days, each of them with n=3

| Conc. (µg/mL) | Av 1 (%) | Error 1(%) | Av 2(%) | Error 2(%) | Av 3 (%) | Error 3 (%) |
|---|---|---|---|---|---|---|
| 0 | 100.00 | 5.86 | 100.00 | 1.27 | 100.00 | 4.36 |
| 10 | 116.64 | 15.46 | 91.02 | 3.00 | 97.35 | 4.52 |
| 50 | 128.14 | 10.08 | 97.72 | 0.99 | 96.14 | 5.06 |
| 250 | 122.77 | 11.96 | 107.66 | 3.00 | 99.91 | 3.23 |
| 500 | 104.61 | 5.15 | 100.28 | 3.58 | 104.49 | 4.20 |

**Table S16:** Macrophage cells viability data upon incubation with MUV-10 28 nm during 72 hours for three different experiments performed on different days, each of them with n=3

| Conc. (µg/mL) | Av 1 (%) | Error 1(%) | Av 2(%) | Error 2(%) | Av 3 (%) | Error 3 (%) |
|---|---|---|---|---|---|---|
| 0 | 100.00 | 5.86 | 100.00 | 1.27 | 100.00 | 4.36 |
| 10 | 108.12 | 6.16 | 93.59 | 0.91 | 95.13 | 4.91 |
| 50 | 119.66 | 12.39 | 96.12 | 1.18 | 95.37 | 9.44 |
| 250 | 129.74 | 9.97 | 98.22 | 1.74 | 96.52 | 4.05 |
| 500 | 123.72 | 19.35 | 95.92 | 1.03 | 92.38 | 4.10 |

### S.7.1.B MTT Essays with Human peripheral blood mononuclear cells

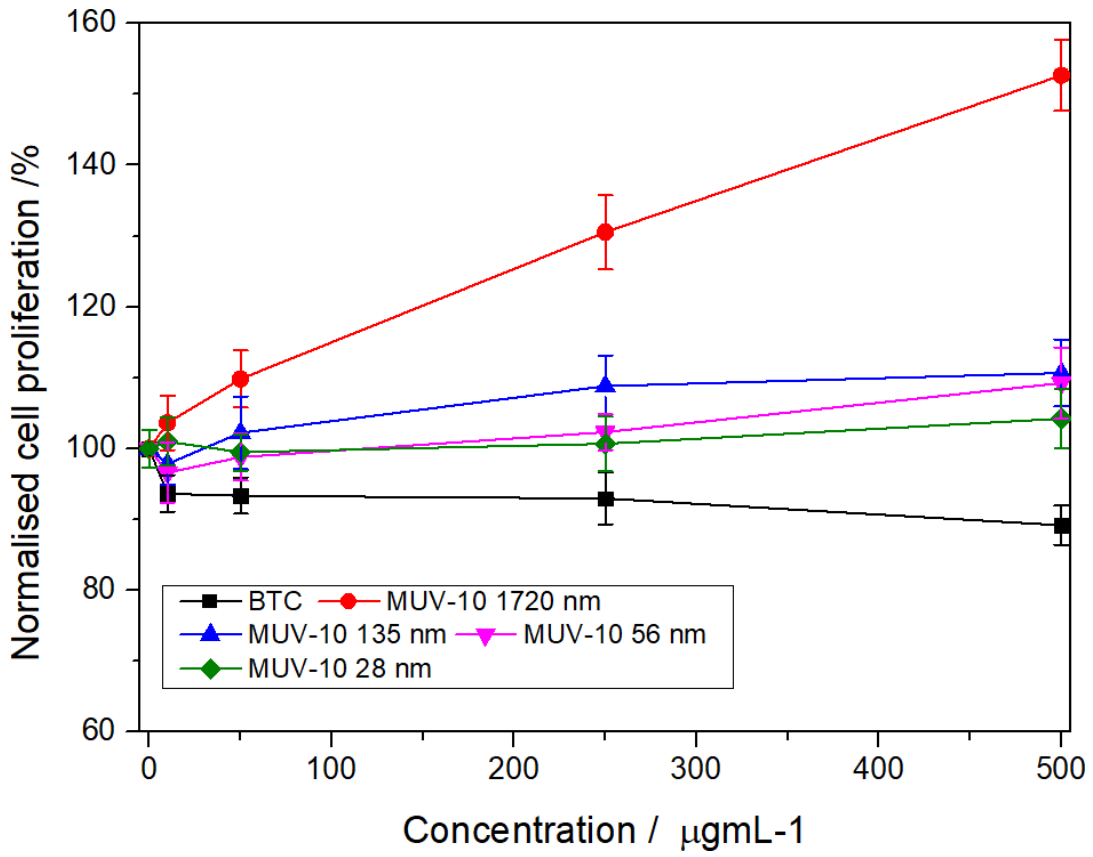


|**Figure S47:** Cytotoxicity of MUV-10 samples measured by MTT assay towards PBM cells isolated from the blood of human donorsafter 24 hours of incubation. (5 independent experiments performed in different days, each of them with n=3)

**Table S17:** Human peripheral blood mononuclear cells viability data upon incubation with BTC during 24 hours for five different experiments performed on different days, each of them with n=3

| Conc. (µg/mL) | Av 1 (%) | Error 1(%) | Av 2(%) | Error 2(%) | Av 3 (%) | Error 3 (%) | Av 4 (%) | Error 4 (%) | Av 5 (%) | Error 5 (%) |
|---|---|---|---|---|---|---|---|---|---|---|
| 0 | 100.00 | 4.33 | 100.00 | 4.00 | 100.00 | 1.01 | 100.00 | 3.25 | 100.00 | 0.73 |
| 10 | 93.23 | 3.33 | 89.67 | 3.33 | 98.03 | 2.96 | 94.70 | 2.55 | 92.60 | 0.71 |
| 50 | 87.75 | 3.88 | 94.26 | 2.90 | 94.28 | 2.12 | 96.27 | 3.08 | 94.22 | 0.73 |
| 250 | 110.16 | 7.08 | 93.92 | 3.34 | 93.58 | 2.56 | 92.78 | 4.44 | 91.56 | 0.77 |
| 500 | 88.90 | 4.13 | 87.44 | 4.05 | 86.76 | 1.10 | 90.13 | 2.14 | 92.66 | 2.30 |

**Table S18:** Human peripheral blood mononuclear cells viability data upon incubation with MUV-10 1720 nm during 24 hours for five different experiments performed on different days, each of them with n=3

| Conc. (µg/mL) | Av 1 (%) | Error 1(%) | Av 2(%) | Error 2(%) | Av 3 (%) | Error 3 (%) | Av 4 (%) | Error 4 (%) | Av 5 (%) | Error 5 (%) |
|---|---|---|---|---|---|---|---|---|---|---|
| 0 | 100.00 | 4.33 | 100.00 | 4.00 | 100.00 | 1.01 | 100.00 | 3.25 | 100.00 | 0.73 |
| 10 | 110.64 | 4.44 | 102.94 | 4.12 | 102.91 | 2.26 | 101.92 | 3.32 | 99.78 | 5.11 |
| 50 | 112.88 | 7.28 | 111.34 | 5.68 | 114.57 | 2.28 | 105.89 | 2.48 | 104.52 | 2.54 |
| 250 | 134.28 | 12.07 | 131.72 | 4.09 | 146.54 | 2.52 | 133.15 | 4.95 | 107.11 | 2.48 |
| 500 | 141.74 | 5.37 | 158.48 | 4.99 | 169.98 | 1.57 | 152.41 | 6.80 | 140.81 | 6.37 |

**Table S19:** Human peripheral blood mononuclear cells viability data upon incubation with MUV-10 135 nm during 24 hours for five different experiments performed on different days, each of them with n=3

| Conc. (µg/mL) | Av 1 (%) | Error 1(%) | Av 2(%) | Error 2(%) | Av 3 (%) | Error 3 (%) | Av 4 (%) | Error 4 (%) | Av 5 (%) | Error 5 (%) |
|---|---|---|---|---|---|---|---|---|---|---|
| 0 | 100.00 | 4.33 | 100.00 | 4.00 | 100.00 | 1.01 | 100.00 | 3.25 | 100.00 | 0.73 |
| 10 | 94.63 | 3.35 | 103.71 | 5.18 | 95.71 | 2.45 | 94.14 | 2.67 | 94.91 | 7.66 |
| 50 | 99.19 | 3.85 | 106.94 | 3.96 | 97.56 | 2.86 | 96.52 | 3.14 | 93.88 | 2.53 |
| 250 | 104.24 | 4.91 | 95.74 | 2.89 | 108.40 | 1.51 | 99.44 | 2.30 | 103.84 | 1.08 |
| 500 | 112.70 | 6.95 | 108.21 | 3.63 | 112.57 | 4.75 | 101.69 | 3.35 | 111.12 | 6.52 |

**Table S20:** Human peripheral blood mononuclear cells viability data upon incubation with MUV-10 56 nm during 24 hours for five different experiments performed on different days, each of them with n=3

| Conc. (µg/mL) | Av 1 (%) | Error 1(%) | Av 2(%) | Error 2(%) | Av 3 (%) | Error 3 (%) | Av 4 (%) | Error 4 (%) | Av 5 (%) | Error 5 (%) |
|---|---|---|---|---|---|---|---|---|---|---|
| 0 | 100.00 | 4.33 | 100.00 | 4.00 | 100.00 | 1.01 | 100.00 | 3.25 | 100.00 | 0.73 |
| 10 | 86.90 | 2.78 | 99.34 | 3.60 | 102.62 | 2.29 | 99.91 | 2.83 | 100.46 | 3.27 |
| 50 | 105.42 | 9.37 | 104.82 | 3.91 | 96.38 | 3.66 | 100.94 | 2.79 | 103.67 | 5.74 |
| 250 | 108.45 | 3.74 | 105.54 | 6.78 | 105.72 | 1.29 | 112.59 | 3.05 | 111.91 | 6.62 |
| 500 | 114.37 | 9.43 | 113.87 | 3.43 | 104.81 | 1.24 | 112.29 | 6.10 | 108.10 | 3.25 |

**Table S21:** Human peripheral blood mononuclear cells viability data upon incubation with MUV-10 28 nm during 24 hours for five different experiments performed on different days, each of them with n=3

| Conc. (µg/mL) | Av 1 (%) | Error 1(%) | Av 2(%) | Error 2(%) | Av 3 (%) | Error 3 (%) | Av 4 (%) | Error 4 (%) | Av 5 (%) | Error 5 (%) |
|---|---|---|---|---|---|---|---|---|---|---|
| 0 | 100.00 | 4.33 | 100.00 | 4.00 | 100.00 | 1.01 | 100.00 | 3.25 | 100.00 | 0.73 |
| 10 | 97.82 | 4.89 | 103.16 | 3.07 | 102.18 | 1.53 | 102.05 | 2.70 | 99.82 | 4.60 |
| 50 | 97.87 | 3.78 | 105.15 | 3.81 | 102.75 | 1.73 | 96.09 | 2.61 | 95.55 | 0.94 |
| 250 | 94.10 | 5.75 | 104.03 | 3.36 | 101.71 | 1.33 | 99.77 | 4.45 | 103.76 | 4.48 |
| 500 | 102.85 | 5.13 | 108.20 | 4.50 | 110.14 | 3.50 | 101.03 | 3.13 | 99.00 | 4.60 |

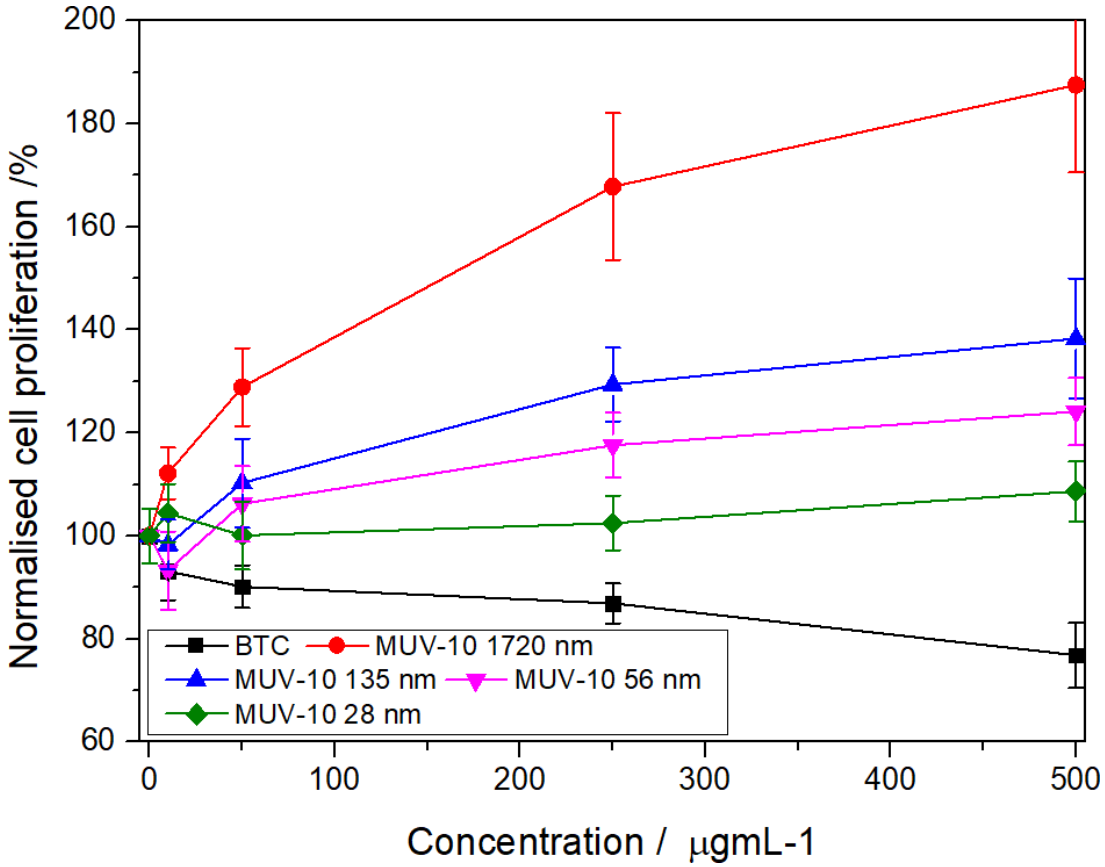


|**Figure S48:** Cytotoxicity of MUV-10 samples measured by MTT assay towards PBM cells isolated from the blood of human donors after 24 hours of incubation. (3 independent experiments performed in different days, each of them with n=3)

**Table S22:** Human peripheral blood mononuclear cells viability data upon incubation with BTC during 72 hours for three different experiments performed on different days, each of them with n=3

| Conc. (ug/mL) | Av 1 (%) | Error 1(%) | Av 2(%) | Error 2(%) | Av 3 (%) | Error 3 (%) |
|---|---|---|---|---|---|---|
| 0 | 100.00 | 8.42 | 100.00 | 3.69 | 100.00 | 3.74 |
| 10 | 103.75 | 6.57 | 81.73 | 5.92 | 93.93 | 4.39 |
| 50 | 100.10 | 7.00 | 81.78 | 2.85 | 88.51 | 2.53 |
| 250 | 98.09 | 6.11 | 81.07 | 2.14 | 81.52 | 3.39 |
| 500 | 91.89 | 6.76 | 64.16 | 4.53 | 74.43 | 7.65 |

**Table S23:** Human peripheral blood mononuclear cells viability data upon incubation with MUV-10 1720 nm during 72 hours for three different experiments performed on different days, each of them with n=3

| Conc. (ug/mL) | Av 1 (%) | Error 1(%) | Av 2(%) | Error 2(%) | Av 3 (%) | Error 3 (%) |
|---|---|---|---|---|---|---|
| 0 | 100.00 | 8.42 | 100.00 | 3.69 | 100.00 | 3.74 |
| 10 | 118.88 | 8.25 | 108.14 | 2.89 | 109.42 | 3.80 |
| 50 | 132.97 | 8.79 | 129.98 | 5.84 | 123.75 | 8.08 |
| 250 | 171.10 | 17.71 | 191.28 | 18.86 | 141.07 | 6.07 |
| 500 | 223.51 | 15.79 | 197.56 | 26.52 | 141.52 | 8.62 |

**Table S24:** Human peripheral blood mononuclear cells viability data upon incubation with MUV-10 135 nm during 72 hours for three different experiments performed on different days, each of them with n=3

| Conc. (ug/mL) | Av 1 (%) | Error 1(%) | Av 2(%) | Error 2(%) | Av 3 (%) | Error 3 (%) |
|---|---|---|---|---|---|---|
| 0 | 100.00 | 8.42 | 100.00 | 3.69 | 100.00 | 3.74 |
| 10 | 108.22 | 7.62 | 90.54 | 3.44 | 96.10 | 3.49 |
| 50 | 127.57 | 14.66 | 102.22 | 3.02 | 101.00 | 8.18 |
| 250 | 130.63 | 8.95 | 141.16 | 8.57 | 116.35 | 3.97 |
| 500 | 147.16 | 17.45 | 145.24 | 12.13 | 122.58 | 5.27 |

**Table S25:** Human peripheral blood mononuclear cells viability data upon incubation with MUV-10 56 nm during 72 hours for three different experiments performed on different days, each of them with n=3

| Conc. (ug/mL) | Av 1 (%) | Error 1(%) | Av 2(%) | Error 2(%) | Av 3 (%) | Error 3 (%) |
|---|---|---|---|---|---|---|
| 0 | 100.00 | 8.42 | 100.00 | 3.69 | 100.00 | 3.74 |
| 10 | 103.51 | 10.86 | 78.94 | 6.15 | 97.33 | 5.80 |
| 50 | 108.01 | 6.71 | 110.45 | 7.33 | 100.26 | 7.93 |
| 250 | 125.57 | 9.65 | 116.44 | 3.62 | 110.77 | 5.54 |
| 500 | 138.80 | 10.63 | 123.54 | 4.88 | 110.09 | 4.15 |

**Table S26:** Human peripheral blood mononuclear cells viability data upon incubation with MUV-10 28 nm during 72 hours for three different experiments performed on different days, each of them with n=3

| Conc. (ug/mL) | Av 1 (%) | Error 1(%) | Av 2(%) | Error 2(%) | Av 3 (%) | Error 3 (%) |
|---|---|---|---|---|---|---|
| 0 | 100.00 | 8.42 | 100.00 | 3.69 | 100.00 | 3.74 |
| 10 | 113.34 | 7.85 | 99.22 | 6.31 | 100.72 | 2.75 |
| 50 | 105.23 | 10.93 | 96.56 | 4.67 | 98.47 | 4.03 |
| 250 | 109.23 | 6.95 | 98.43 | 3.44 | 99.80 | 5.50 |
| 500 | 113.40 | 8.22 | 106.57 | 4.38 | 105.96 | 4.89 |

### S.7.2. Reactive Oxygen Species (ROS) Production

ROS production assays were carried out as described in **Section S.3.4**, using solutions with 0.25 mg/mL of MOF. Macrophages N=3

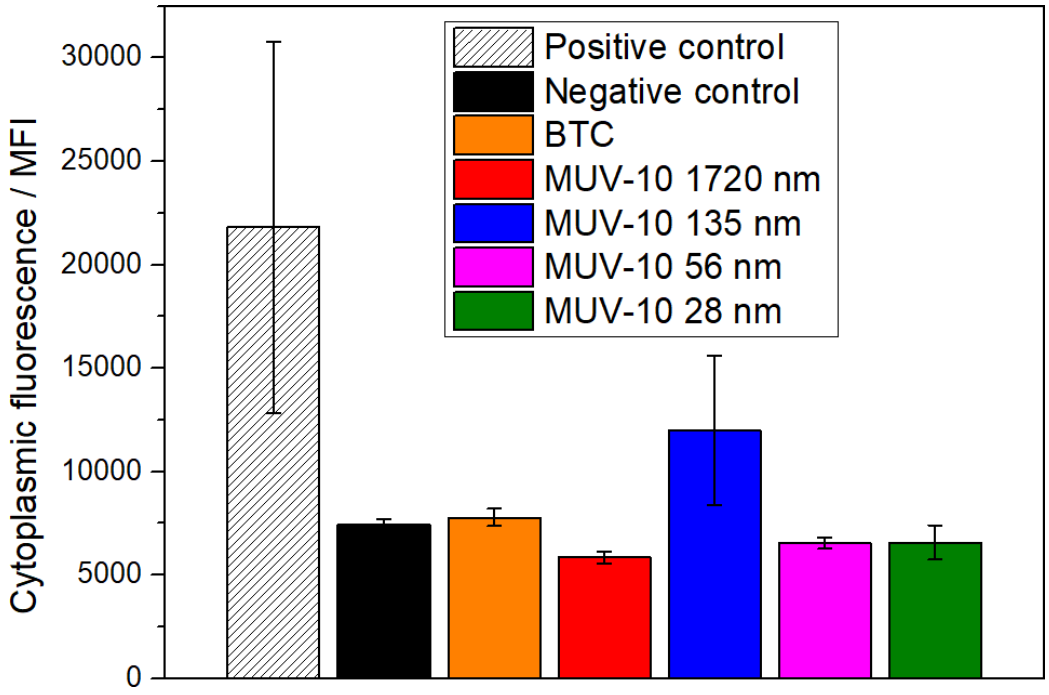


|**Figure S49:** Reactive oxygen species (ROS) generation in J774 macrophage cells on exposure to MUV-10 MOFs.

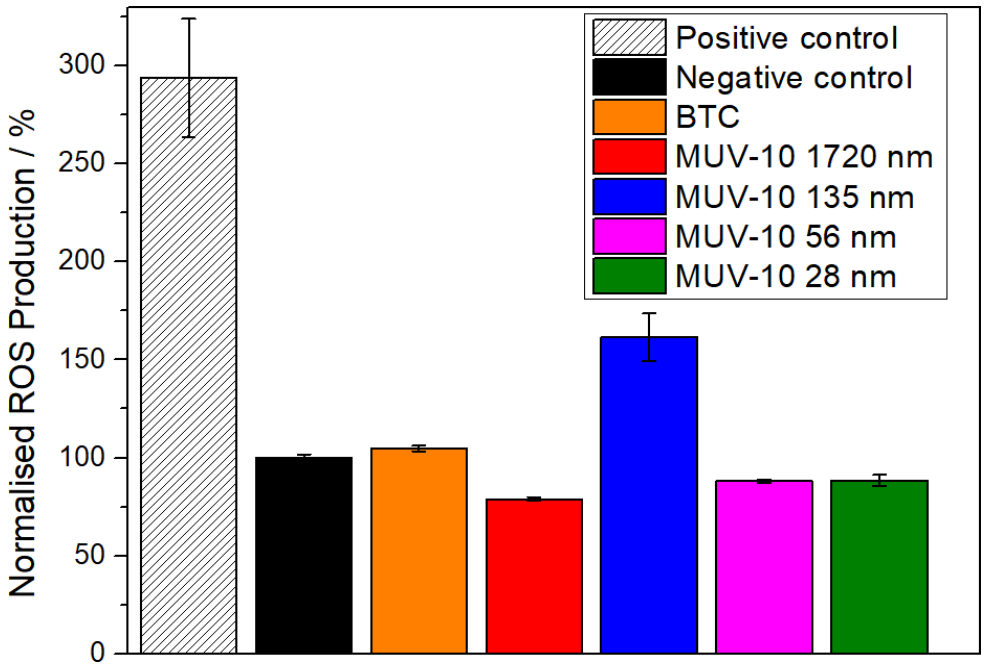


|**Figure S50:** Normalised Reactive oxygen species (ROS) generation in J774 macrophage cells on exposure to MUV-10 MOFs.

## S7.3. Human Immune System Response Towards MUV-10

The individual data for immune system response in serum derived from four human patients are detailed in the following figures for C3 and C4 complement cascade activation **(See Section S3.5).**

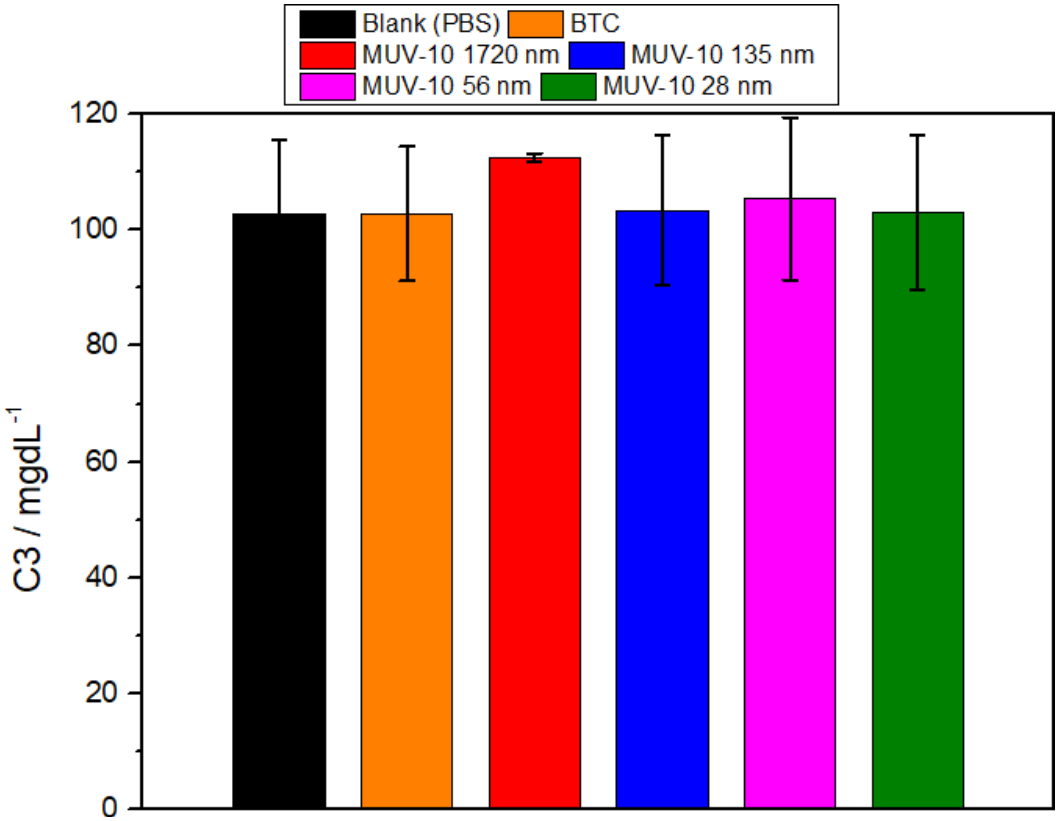


|**Figure S51:** Complement cascade activation in human blood plasma induced by incubation with MUV-10 samples, plotted for production of C3 complement component, averaged from blood samples from five human donors.

**Table S27:** C3 concentration (mg/dL) of the blood plasma from different human donnors upon treatment with 250 µg/mL of the MUV-10 samples.

| **C3 (mg/dL)** | | | | | | |
|---|---|---|---|---|---|---|
| **Donor** | **C-(PBS)** | **BTC** | **1720 nm** | **135 nm** | **56 nm** | **28 nm** |
| **1** | 111 | 109 | 112 | 109 | 114 | 112 |
| **2** | 108 | 111 | 113 | 112 | 112 | 110 |
| **3** | 111 | 109 | | 111 | 114 | 110 |
| **4** | 81 | 83 | | 81 | 81 | 80 |
| **5** | 103 | 102 | | 104 | 106 | 103 |

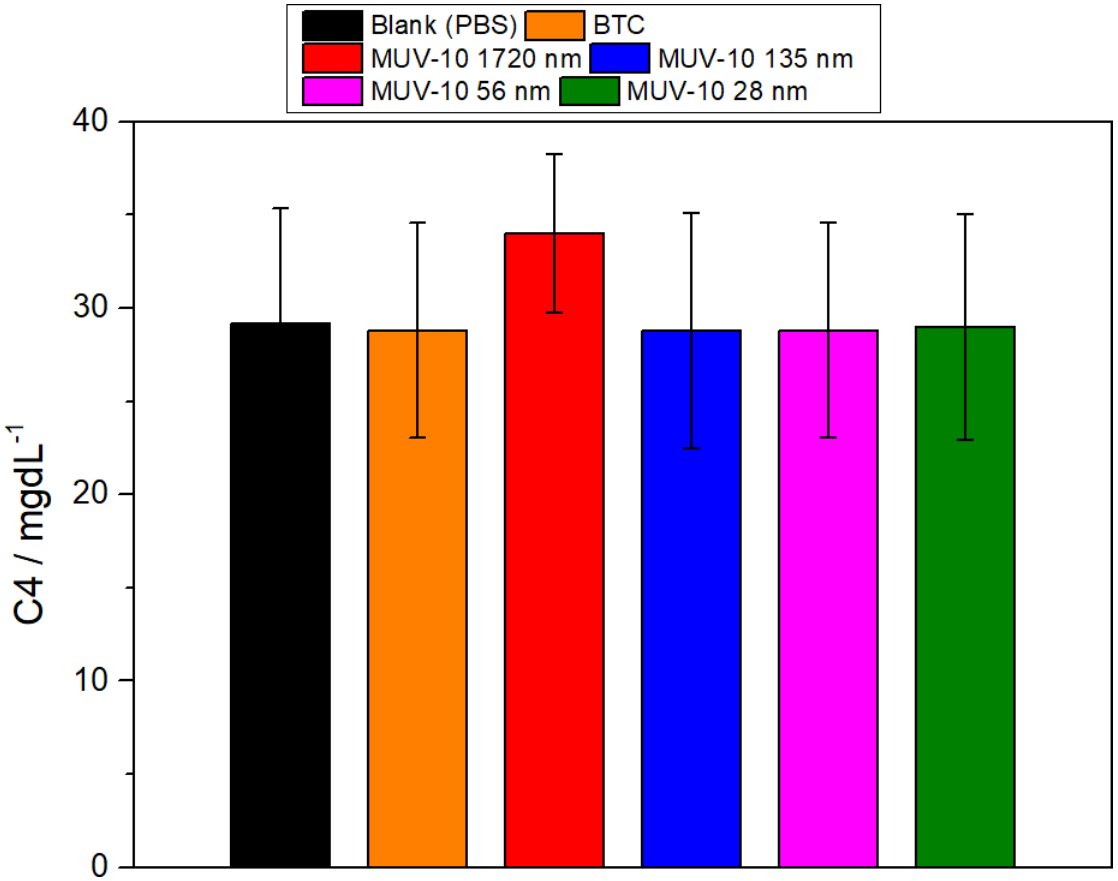


|**Figure S52:** Complement cascade activation in human blood plasma induced by incubation with MUV-10 samples, plotted for production of C4 complement component, averaged from blood samples from five human donors.

**Table S28:** C4 concentration (mg/dL) of the blood plasma from different human donors upon treatment with 250 µg/mL of the MUV-10 samples

| **C4 (mg/dL)** | | | | | | |
|---|---|---|---|---|---|---|
| **Donor** | **C-(PBS)** | **BTC** | **1720 nm** | **135 nm** | **56 nm** | **28 nm** |
| **1** | 32 | 32 | 31 | 32 | 32 | 31 |
| **2** | 37 | 36 | 37 | 37 | 36 | 37 |
| **3** | 31 | 30 | | 30 | 30 | 31 |
| **4** | 24 | 24 | | 23 | 24 | 24 |
| **5** | 22 | 22 | | 22 | 22 | 22 |

## References

(1) Abánades-Lázaro, I.; Almora-Barrios, N.; Tatay, S.; Martí-Gastaldo, C. Effect of Modulator Connectivity on Promoting Defectivity in Titanium–Organic Frameworks. *Chem Sci* **2020**, *12*, 2586-2593 . https://doi.org/10.1039/d0sc06105k.

(2) Abánades-Lázaro, I. A Comprehensive Thermogravimetric Analysis Multifaceted Method for the Exact Determination of the Composition of Multi-functional Metal-Organic Framework Materials. *Eur J Inorg Chem* **2020,** *2020*, 4284-4294.. https://doi.org/10.1002/ejic.202000656.